Available online at www.sciencedirect.com
SCIENCE DIRECT®
Journal of Computational Physics 209 (2005) 754–786
JOURNAL OF COMPUTATIONAL PHYSICS
www.elsevier.com/locate/jcp

Higher order corrections in the approximation of low-dimensional manifolds and the construction of simplified problems with the CSP method

Mauro Valorani [a,*], Dimitris A. Goussis [b], Francesco Creta [a], Habib N. Najm [c]

[a] *Dipartimento di Meccanica e Aeronautica, University of Rome La Sapienza, Via Eudossiana 18, 00184 Rome, Italy*
[b] *Agiou Georgiou 49, 26500 Patra, Greece*
[c] *Sandia National Laboratories, Livermore, CA 94551, United States*

Received 26 October 2004; received in revised form 30 March 2005; accepted 30 March 2005
Available online 1 June 2005

Abstract

In systems of stiff Ordinary Differential Equations (ODEs) both fast and slow time scales are encountered. The fast time scales are responsible for the development of low-dimensional manifolds on which the solution moves according to the slow time scales. In this paper, methodologies for constructing highly accurate (i) expressions describing the manifold, and (ii) simplified non-stiff equations governing the slow evolution of the solution on the manifold are developed, according to an iterative procedure proposed in the Computational Singular Perturbation (CSP) method. It is shown that the increasing accuracy achieved with each iteration is directly related to the time rates of change of the CSP vectors spanning the manifold along the solution trajectory. Here, an algorithm is presented which implements these calculations and is validated on the basis of two simple examples.

PACS: 82.40.g; 02.40.Vh; 02.60.Lj

Keywords: Chemical kinetics and reactions; Slow invariant manifold; Ordinary differential equation

* Corresponding author. Tel.: +39 06 4458 5278; fax: +39 06 483 729.
E-mail address: m.valorani@dma.ing.uniroma1.it (M. Valorani).
URL: macprop2.ing.uniroma1.it/valorani (M. Valorani).

0021-9991/$ - see front matter © 2005 Elsevier Inc. All rights reserved.
doi:10.1016/j.jcp.2005.03.033

1. Introduction

In spite of the rapid and significant increase in computing power of current processors and parallel computational architectures, the numerical solution of multi-scale problems (chemical kinetics, biological modeling, atmospheric prediction, control, electronics, etc.) remains a daunting task, mostly because the time scales of interest are usually much slower than the fastest time scales characterizing this class of systems. The mathematical models which attempt at reproducing this phenomenology, are usually classified as being "stiff".

Stiffness can indeed be associated with a spread in the magnitude of (i) the real, negative part of the eigenvalues of the system, and/or (ii) their imaginary part; the first category being associated with the presence of dissipative processes, such as viscous dissipation and/or chemical reactions, and the latter to nonlinear convective transport or nonlinear oscillatory behavior. In this work, we will consider stiff systems of dissipative nature only, that is systems characterized by a number of eigenvalues with a dominant negative real part, or more in general by characteristic time scales providing a fast exponential relaxation of the processes associated with these fast time scales.

Stability requires explicit schemes of integration to advance the numerical solution of a stiff problem with time steps of the order of the fastest scale, whereas the time scale of interest can be several orders of magnitude slower. This makes the numerical integration exceedingly inefficient. A standard approach to circumvent the stability constraint is to adopt implicit schemes of integration, among which the family of BDF schemes due to Gear [1] remains the most widely adopted. These schemes have been incorporated in very successful software libraries (LSODE, DVODE, etc. [2–4]).

The occurrence of time scales much faster than the one of interest is what makes stiff problems difficult to solve. On the other hand, it also paves an alternate route to the adoption of implicit schemes, in order to circumvent the stability constraints of explicit schemes. In fact, given an N-dimensional problem, where N might be the number of species in a chemical mechanism, the role of the fast scales in the dynamics of a stiff problem is to constrain the point dynamics within a hypersurface with a dimension lower than N, thus effectively reducing the number of degrees of freedom left available. Therefore, the solution of the stiff problem can be sought by constructing a reduced model, approximating the original one, such that it describes just the point dynamics restricted within this low-dimensional hypersurface. The reduced model will be of lower dimension and free from the fast scales, as compared to the original one. Ultimately, the construction of the reduced model requires an accurate identification of the low-dimensional hypersurface.

In chemical kinetics, the use of the Steady-State Approximation (SSA) [5,6] was one of the first attempts to follow this concept. SSA has been accepted widely, even though its theoretical foundations, domain of applicability, and ease of use, have been questioned since its inception [7–9].

The theoretical foundations supporting SSA have been reconsidered in Fraser [10], who adopted a geometrical framework to discuss the different approximations of the dynamics of stiff systems. Fraser pointed out that the reduced model as identified by SSA must be described as consisting of (i) a lower-dimensional hypersurface $\mathbf{S}$ in the phase space of the system, and (ii) a set of non-stiff ODEs describing the evolution of the non-steady-state species which is constrained to occur in $\mathbf{S}$. The hypersurface $\mathbf{S}$ is identified by the set of algebraic equations obtained by enforcing that, for some selected ("steady-state") species, the RHS of the original set of ODEs be identically zero.

The SSA had three major flaws, namely (i) it is difficult to identify the correct set of steady-state (SS) species, (ii) the trajectory flow – defined as the set of all possible trajectories satisfying the stiff ODEs – of the system is not attracted by the hypersurface defined by SSA, but by a different low-dimensional hypersurface, and (iii) the SS species and the related hypersurface might be time dependent.

Fraser showed that, for the class of stiff (dissipative) systems, the trajectory flow undergoes a strong contraction, that is trajectories tend to approach one another as time increases, onto a low-dimensional (smooth) hypersurface in the N-dimensional phase space, which lies close to the SSA surface (a reason

justifying the partial success of SSA) and yet different from it. The hypersurface asymptotically attracting all trajectories is usually referred to as the Slow Invariant Manifold (SIM) of the stiff system.

A rigorous mathematical definition of a SIM can be found in [11] for the class of singularly perturbed dynamical systems. The Fenichel theory establishes the existence of a SIM for problems involving a wide temporal gap between slow and fast dynamics. This SIM is characterized by being both (i) an invariant of the dynamics and (ii) exponentially attractive for the trajectory flow.

The complexity of the problems of interest today motivated research on the development of algorithms for the computational identification of SIMs. From these activities, two broad classes of approaches emerged, one aimed at identifying the locus of the points in the phase space belonging to the SIM, the other attempting at identifying both the SIM hypersurface and the main geometrical properties of the SIM, i.e. its invariant subspaces and the characteristic time scales associated with them.

The method due to Fraser [10] belongs to the first class of approaches, with further developments by Roussel and Fraser [12]. It involves an iterative scheme to find the SIM as the fixed point, in the function space, of a contraction mapping of the invariance equation associated with the dynamical system. The procedure is explicit if the system is linear in the fast variable(s), and implicit otherwise; thus involving the solution of a nonlinear set of equations to find the SIM geometry numerically. Under proper conditions, this method yields, term by term, the correct asymptotic expansion of the SIM [13].

The procedure proposed in [12], besides requiring the definition of the proper parametrization of the SIM, does not always converge for an infinite number of iterations, and might indeed diverge when the curvature of the manifold is too high [12].

In this regard, Davis and Skodje [14] proposed a faster-converging variant of the Roussel–Fraser algorithm that involved the addition of a pseudo-time derivative to the functional equation. A different approach to stabilize Fraser's iterations was pointed out by Roussel [15], who suggested the modification of the functional equation according to a mapping which circumvents the convergence failures while leaving the fixed point unaltered. Nafe and Maas [16] proposed an extension of the relaxation procedure introduced by Davis and Skodje [14], which involves the solution of a set of (pseudo) time dependent nonlinear PDEs, defined in the phase space of the m parameters. This procedure, starting from a proper initial guess – say the m-dimensional Intrinsic Low-Dimensional Manifold (ILDM), finds the correct SIM at large times.

The Computational Singular Perturbation (CSP) method, co-developed by Lam and Goussis [17–22], belongs to the second class of approaches. Given an N-dimensional problem, CSP provides a geometrical description of the SIM, by identifying the set of "fast" basis vectors, A_r, and the corresponding set of dual vectors, B^r, spanning the M-dimensional "fast" subspace (with $M < N$), which is locally orthogonal to the $(N - M)$-dimensional SIM.

The essential part of the CSP method involves an iterative procedure, specifically designed to identify the basis vectors that span the two subdomains, where the fast and slow time scales act, respectively; the latter subdomain being identical to the SIM. The process starts with an arbitrary initial guess for the "fast" basis vectors A_r, that eventually will span the fast subdomain, and their dual B^r. After each iteration, better approximations of the "fast", and its complementary "slow", subspaces are obtained. There exist two types of iterations which are independent of each other: the A_r- and B^r-refinement procedures. The B^r-refinement increases the accuracy in the description of the SIM, by better approximating the "fast" subspace, while, the A_r-refinement makes the simplified problem non-stiff by better approximating the "slow" subspace. Seen from a different point of view, the B^r-refinement decreases the influence of the slow time scales on the computed approximation of the "fast" subspace, while each A_r-refinement decreases the influence of the fast time scales on the computed approximation of the "slow" subspace.

At each iteration, the improvement in the approximation of the A_r and B^r basis vectors is achieved by taking into account the geometrical characteristics of the manifold (such as local curvature and higher order terms). The accuracy improves at each iteration by a factor of the order of ε, the small parameter in the singular perturbation expansion of the CSP method.

The successive approximations of the basis vectors, obtained after each CSP iteration, converge (i) to the local eigenvectors of the Jacobian matrix of the dynamical system if the contribution of the higher order terms, quantified in the refinement formulae by the time rates of change of the basis vectors, is neglected, yielding a leading order approximation of the SIM, or (ii) to the correct asymptotic representation of the SIM, in powers of ε, if this contribution is accounted for [23].

As "fast" basis vectors, the ILDM method of Maas and Pope [24–26] selects the right and left eigenvectors of the local Jacobian of the problem flow associated with the negative eigenvalues with the largest absolute value of the real part.[1] This choice of basis vectors makes ILDM exact only for linear problems, and for nonlinear problems in the limit of a vanishingly small time scale separation ε [13,23]. According to the ILDM method, the SIM is generated and stored as a look-up table, and this requires the prescription of the SIM's dimension a priori as a constant throughout the phase space.

As previously noted, CSP provides high-order accuracy for a nonlinear problem by following a rather straightforward procedure, the CSP refinements, which involve the time rates of change of the CSP vectors. Whereas the CSP refinements have been introduced long ago [18,20], no specific analysis has been carried out yet on how to evaluate the time rates of change of the CSP vectors. Moreover, although the CSP method has been adopted in several investigations (e.g. [27–31]), the higher order effects have never been examined due to the lack of a reliable method for computing the time rates of change of the CSP vectors. As a matter of fact, their calculation is straightforward when the analytic expressions of the basis vectors can be obtained, for example with the help of a symbolic manipulator. This is, for example, the case in the Davis and Skodje model [14] analyzed by Zagaris et al. in [23] to study the asymptotic properties of the CSP method. When the analytic expressions of the basis vectors cannot be obtained, then one could envisage computing the time rates of change of the CSP vectors by finite differences evaluated along a trajectory path. However, eigenvalue crossings alter the ordering of the vectors and require an explicit tracking of the time evolution of the vectors. Moreover, what really matters is the time rate of change of the fast subspace, and not quite the rotation of the individual vectors.

In the present work, we provide explicit formulae for the calculation of the time rates of change of the CSP vectors for a general nonlinear problem. These formulae show that the computation of the time rates of change of the CSP vectors requires the calculation of the time rate of change of the Jacobian matrix of the RHS of the original ODEs ($\mathrm{d}J/\mathrm{d}t$, $\mathrm{d}^2J/\mathrm{d}t^2$, ...). They also show that these terms depend on the state of the system only, being local measures of the geometrical characteristics of the manifold (such as local curvature and higher order terms), as they involve the terms $\partial J/\partial y^i$, $\partial^2 J/\partial y^i \partial y^j$, ...

As a consequence, the time rates of change of the CSP vectors also depend exclusively on the local state variables, as well as the local Jacobian matrix and the SIM dimension. Hence, all SIMs properties can be stored in look-up tables, generated by tabulation methods like PRISM [32] or ISAT [33], possibly in conjunction with the development of efficient explicit schemes of integration of stiff problems based upon a time-scale splitting [30,34].

We will verify, with reference to two model problems, the validity of the formulae for the calculation of the time rates of change of the CSP vectors. The first model problem is a planar ODE with an explicit, constant, small parameter and prescribed slow and fast variables. It has been proposed and discussed by Davis and Skodje [14], and reconsidered by Kaper and Kaper in [13]. Among other features, the Davis and Skodje model possesses an exact representation of the manifold, a circumstance enabling us to obtain unambiguous error estimates. For this model problem, the time rates of change of the CSP vectors can be obtained in closed form.

The second model problem describes the kinetics of a 3-species model chemical system, which mimicks more realistic chemical mechanisms, possibly involving many tens of species and hundreds of reactions,

[1] The basis vectors in the first versions of ILDM were obtained by a Schur decomposition of the Jacobian, which in most cases is equivalent to the choice of the right/left eigenvectors of the Jacobian as the bases in the tangent/cotangent spaces.

characterized by having a non-constant, non-explicitly defined small parameter and non-prescribed slow and fast variables. Moreover, the CSP vectors and their time rates of change are sufficiently simple that they can still be evaluated algebraically, but complicated enough so as to allow a non-trivial validation of the procedures for the CSP refinements.

The manuscript is organized as follows. First, a brief outline of the basic CSP concepts will be presented in Section 2, as it is relevant to the present analysis; a more detailed presentation of the CSP method can be found in [18–21] for the case of ODEs and in [19,35,31] for the case of PDEs. The specific details of the implementation of the CSP refinements when the time rates of change of the CSP vectors are retained are illustrated in Sections 3 and 4. Finally, the results of the method as applied to the two model problems are reported and discussed in Sections 5 and 6 to explain the different features of the method and the means by which high accuracy results are obtained.

2. Basic CSP concepts

We consider the evolution of a physical process governed by a system of N ordinary differential equations of the form:

$$\frac{\mathrm{d}\boldsymbol{y}}{\mathrm{d}t} = \boldsymbol{g}(\boldsymbol{y}), \tag{1}$$

where $\boldsymbol{y}$ is the N-dimensional vector of the dependent variables and $\boldsymbol{g}$ is an algebraic function of $\boldsymbol{y}$. It is assumed that Eq. (1) is stiff; i.e. some of the fastest time scales in the problem are much faster than the time scales of interest.

Following the CSP method, at each point in the phase space, the vector $\boldsymbol{g}$ can be decomposed in two components by projecting it onto the M-dimensional fast and the $(N - M)$-dimensional slow subspaces (i.e., the subspaces where the fast and slow time scales act, respectively) spanned by the CSP vectors $\boldsymbol{a}_i$ ($i = 1, M$) and $\boldsymbol{a}_j$ ($j = M + 1, N$), which can be collected in the $N \times M$ and $N \times (N - M)$-dimensional matrices $A_r(k, m)$ and $A_s(k, m)$ defined as follows:

$$\begin{aligned} A_r(k,m) &= [\boldsymbol{a}_1(k,m), \ldots, \boldsymbol{a}_M(k,m)], \\ A_s(k,m) &= [\boldsymbol{a}_{M+1}(k,m), \ldots, \boldsymbol{a}_N(k,m)], \end{aligned} \tag{2}$$

where k and m denote the levels of two kinds of refinement, to be discussed next. Each basis vector $\boldsymbol{a}_i$ (or mode) is associated with a time scale acting along the corresponding direction. The modes are ordered according to their speed; the first mode associated with the fastest scale and the last with the slowest.

Let a second set of CSP basis vectors defined by $\boldsymbol{b}^i$ ($i = 1, M$) and $\boldsymbol{b}^j$ ($j = M + 1, N$), which are collected in the $M \times N$ and $(N - M) \times N$-dimensional matrices $B^r(k, m)$ and $B^s(k, m)$:

$$B^r(k,m) = \begin{bmatrix} \boldsymbol{b}^1(k,m) \\ \boldsymbol{b}^2(k,m) \\ \vdots \\ \boldsymbol{b}^M(k,m) \end{bmatrix}, \quad B^s(k,m) = \begin{bmatrix} \boldsymbol{b}^{M+1}(k,m) \\ \boldsymbol{b}^{M+2}(k,m) \\ \vdots \\ \boldsymbol{b}^N(k,m) \end{bmatrix}. \tag{3}$$

The $\boldsymbol{b}^i$ vectors are the duals of the $\boldsymbol{a}_i$ vectors. Thus, due to orthogonality, the four matrices satisfy the relations:

$$\begin{aligned} B^r(k,m)A_r(k,m) &= I_M^M, & B^r(k,m)A_s(k,m) &= 0_{N-M}^M, \\ B^s(k,m)A_r(k,m) &= 0_M^{N-M}, & B^s(k,m)A_s(k,m) &= I_{N-M}^{N-M} \end{aligned} \tag{4}$$

and

$$A_r(k,m)B^r(k,m) + A_s(k,m)B^s(k,m) = I_N^N, \tag{5}$$

where I_v^v is the v-dimensional unit matrix and 0_v^u is the $u \times v$ zero matrix.

Projecting the RHS of Eq. (1) onto the fast and slow subspaces yields

$$\frac{\mathrm{d}\boldsymbol{y}}{\mathrm{d}t} = A_r(k,m)\boldsymbol{f}^r(k,m) + A_s(k,m)\boldsymbol{f}^s(k,m), \tag{6}$$

where the M and $(N-M)$-dimensional vectors $\boldsymbol{f}^r(k,m)$ and $\boldsymbol{f}^s(k,m)$ are defined as

$$\boldsymbol{f}^r(k,m) = \begin{bmatrix} f^1(k,m) \\ f^2(k,m) \\ \vdots \\ f^M(k,m) \end{bmatrix}, \quad \boldsymbol{f}^s(k,m) = \begin{bmatrix} f^{M+1}(k,m) \\ f^{M+2}(k,m) \\ \vdots \\ f^N(k,m) \end{bmatrix}, \tag{7}$$

and where each mode amplitude f^i is defined as

$$f^i(k,m) = \boldsymbol{b}^i(k,m) \cdot \boldsymbol{g}. \tag{8}$$

Where, in the phase space, the amplitudes of the M fastest modes attain negligible magnitude, i.e. the following algebraic equations hold:

$$\boldsymbol{f}^r(k,m) = B^r(k,m)\boldsymbol{g} \approx 0_1^M, \tag{9}$$

then Eq. (9) describe the SIM's shape which has dimension $(N-M)$. There, the corresponding M fast scales have no role anymore in the point dynamics and the locally characteristic time scale is a slow one. This means that the point dynamics cannot move along a trajectory with a component in the "fast" directions $\boldsymbol{a}_i$ $(i = 1, M)$, being thus restricted to move only along the "slow" ones $\boldsymbol{a}_j$ $(j = M+1, N)$; i.e. along the SIM, according to the equations:

$$\frac{\mathrm{d}\boldsymbol{y}}{\mathrm{d}t} \approx A_s(k,m)\boldsymbol{f}^s(k,m) = [I - A_r(k,m)B^r(k,m)]\boldsymbol{g}, \tag{10}$$

where the orthonormality condition, Eq. (5), has been employed in the derivation of the second equality. This simplified system is not stiff, since the modes associated with the M fastest time scales are ignored.

As Eqs. (9) and (10) show, for the construction of both the equation describing the manifold and the simplified problem, it is sufficient to have available the fast basis vectors A_r and B^r only.

As mentioned previously, there are two kinds of CSP refinements. One kind alters B^r and A_s (defined as the B^r-refinement), leaving B^s and A_r unaffected, and is related to the accuracy in the description of the manifold [18,20]. The other kind alters A_r and B^s (defined as the A_r-refinement), leaving B^r and A_s unaffected, and is related to the non-stiffness of the simplified problem [18,20]. Any number of B^r- (or A_r-) refinements can be carried out, independently of the A_r- (or B^r-) refinements. These two kinds of refinements are performed through the relations:

$$B^r(k_1+1,m_1) = T_r^r(k_1,m_1)\left(\frac{\mathrm{d}B^r(k_1,m_1)}{\mathrm{d}t} + B^r(k_1,m_1)J\right), \tag{11}$$

$$A_r(k_1+1,m_1) = A_r(k_1,m_1), \tag{12}$$

$$B^s(k_1+1,m_1) = B^s(k_1,m_1), \tag{13}$$

$$A_s(k_1+1,m_1) = [I - A_r(k_1+1,m_1)B^r(k_1+1,m_1)]A_s(k_1,m_1), \tag{14}$$

where

$$T_r^r(k_1,m_1) = \left[\Lambda_r^r(k_1,m_1)\right]^{-1} = \left[\left(\frac{\mathrm{d}B^r(k_1,m_1)}{\mathrm{d}t} + B^r(k_1,m_1)J\right)A_r(k_1,m_1)\right]^{-1}, \tag{15}$$

and

$$A_r(k_2,m_2+1) = \left[-\frac{\mathrm{d}A_r(k_2,m_2)}{\mathrm{d}t} + JA_r(k_2,m_2)\right]T_r^r(k_2,m_2), \tag{16}$$

$$B^r(k_2,m_2+1) = B^r(k_2,m_2), \tag{17}$$

$$B^s(k_2,m_2+1) = B^s(k_2,m_2)[I - A_r(k_2,m_2+1)B^r(k_2,m_2+1)], \tag{18}$$

$$A_s(k_2,m_2+1) = A_s(k_2,m_2), \tag{19}$$

where

$$T_r^r(k_2,m_2) = \left[\Lambda_r^r(k_2,m_2)\right]^{-1} = \left[\left(\frac{\mathrm{d}B^r(k_2,m_2)}{\mathrm{d}t} + B^r(k_2,m_2)J\right)A_r(k_2,m_2)\right]^{-1}, \tag{20}$$

and k_i and m_i denote the number of B^r- and A_r-refinements, respectively, already performed. The subscript i was introduced here in order to indicate that any number of A_r- or B^r-refinements can precede one additional B^r- or A_r-refinement; the matrix T_r^r being updated accordingly. Of course, both kinds of refinement (11)–(15) and (16)–(20) preserve the orthonormality of the CSP vectors, Eqs. (4) and (5). As mentioned in the introduction, the B^r- and A_r-refinements, respectively, decrease the influence of the slow and fast time scales on the computed approximation of the "fast" and "slow" subspaces at the (k, m)-th level. As a result, the contamination of the amplitudes in $\boldsymbol{f}^r$ and $\boldsymbol{f}^s$, respectively, by the slow and fast time scales will decrease. This development will allow the fast time scales to drive $\boldsymbol{f}^r$ to even smaller values and will reinforce the control of the slow time on the evolution of $\boldsymbol{f}^s$, making the simplified problem, as stated by Eqs. (9) and (10), more accurate and non-stiff. Details on these effects of the A_r- or B^r-refinements are discussed in Appendix A.

If the time derivative terms in Eqs. (11), (15), (16) and (20) are ignored, the iterative formulae of the block power method for the approximation of the left (Eqs. (11)–(14)) and right (Eqs. (16)–(19)) eigenvectors of a matrix are recovered [36–38]. In particular, without the time derivative terms, a set of M arbitrary vectors (column or row) will improve the approximation of the subspace spanned by the M eigenvectors (right or left) corresponding to the M largest eigenvalues of J (in magnitude), by a factor of $\varepsilon = |\lambda(M+1)/\lambda(M)|$ after each (A_r- or B^r-) refinement, where λ(i) is the eigenvalue with the i-th largest magnitude and $\varepsilon < 1$. The smaller the values of ε, the higher the rate of convergence.

The appearance of the time derivative terms in Eqs. (11)–(15) and (16)–(19) is associated with the ability of the CSP vectors to capture the nonlinear effects, by following the rotation in time of the basis vectors spanning the fast and slow subspaces. In principle, one can carry out any number of B^r- and/or A_r-refinements. However, for practical situations, computing the time derivatives in Eqs. (11), (15), (16) and (20) is not a straightforward procedure. Their direct numerical computation along a solution trajectory is excluded, since such an approach cannot handle the case where corresponding eigenvalues cross each other and the ordering of the CSP vectors changes in time. Yet, the time derivatives can be evaluated:

(i) when the analytic expressions of the basis vectors can be obtained, for example with the help of a symbolic manipulator; in this case the time derivatives of $\boldsymbol{a}$ and $\boldsymbol{b}$ can be directly evaluated as

$$\frac{\mathrm{d}\boldsymbol{a}_j}{\mathrm{d}t} = \sum_{i=1,N} \frac{\partial \boldsymbol{a}_j}{\partial y^i} g^i, \tag{21}$$

$$\frac{\mathrm{d}\boldsymbol{b}^j}{\mathrm{d}t} = \sum_{i=1,N} \frac{\partial \boldsymbol{b}^j}{\partial y^i} g^i \tag{22}$$

for any number of refinements, since the partial derivatives $\partial \boldsymbol{a}_j/\partial y^i$ and $\partial \boldsymbol{b}^j/\partial y^i$ can be computed analytically.

(ii) when the analytic expressions of the basis vectors cannot be obtained, typically when the number of unknowns is larger than 3–4, then the time derivatives can be evaluated for a limited number of refinements as discussed in the following two sections.

3. Implementation of CSP refinements

The implementation of the CSP vector procedure, discussed here, can be defined as composed of two phases: (1) a first refinement, wherein the time derivatives of the basis vectors are neglected, yielding leading order accuracy and (2) a second refinement, wherein the time derivatives are included, providing higher order accuracy.

Phase (1) is identical to one block-power refinement and, if carried out many times, the M fast and $N - M$ slow basis vectors will span the two subspaces, the M fast and $N - M$ slow eigenvectors of J, respectively. Considering a nonlinear source term in Eq. (1), additional (more than one) refinements can easily be performed, but are ineffective in improving the leading order accuracy. On the other hand, Phase (2) can practically be carried out just once, providing second order accuracy. This limitation is due to the increasing cost of obtaining higher order time derivatives of the basis vectors needed in further refinements.

Each of the two phases is composed of two steps which, as previously said, are referred to as B^r-refinement (step 1, identified by index k) and A_r-refinement (step 2, identified by index m), respectively. Formulae for the evaluation of $B^r(k, m)$ and $A_r(k, m)$ for $k = 1, 2$ and $m = 1, 2$ are presented below together with expressions for the necessary basis vector time derivatives.

3.1. Phase (1)

Consider the case where the first guess for the refinement procedure of the CSP basis vectors $B^r(0, 0)$ and $A_r(0, 0)$ is a set of arbitrary vectors with

$$\frac{\mathrm{d}B^r(0,\ 0)}{\mathrm{d}t} = 0, \quad \frac{\mathrm{d}A_r(0,\ 0)}{\mathrm{d}t} = 0. \tag{23}$$

3.1.1. Step 1: the B^r-refinement

Under the assumptions (23), the B^r-refinement yields

$$\begin{aligned}
&\lambda_r^r(0,0) = B^r(0,0) J A_r(0,0),\\
&\tau_r^r(0,0) = \left(\lambda_r^r(0,0)\right)^{-1},\\
&B^r(1,0) = \tau_r^r(0,0) B^r(0,0) J,\\
&A_r(1,0) = A_r(0,0),\\
&B^s(1,0) = B^s(0,0),\\
&A_s(1,0) = [I - A_r(1,0)B^r(1,0)]A_s(0,0) = [I - A_r(0,0)B^r(1,0)]A_s(0,0).
\end{aligned}$$

The end effect of step 1 is to lower the norm of the upper-right off-diagonal block:

$$\lambda_s^r(1,0) = B^r(1,0)JA_s(1,0) = \mathrm{O}\left(\varepsilon\lambda_s^r(0,0)\right)$$

by an order $\varepsilon = |\tau_M/\tau_{M+1}| < 1$ (where τ_M and τ_{M+1} are defined in Appendix A, Eq. (A.23)), thereby making the fast modes "purer" by decoupling them from the slow modes, while the lower left off-diagonal block is left unchanged:

$$\lambda_r^s(1,0) = B^s(0,0)JA_r(0,0) = \lambda_r^s(0,0).$$

3.1.2. Step 2: the A_r-refinement

The A_r-refinement yields

$$\lambda_r^r(1,0) = B^r(1,0)JA_r(0,0),$$
$$\tau_r^r(1,0) = \left(\lambda_r^r(1,0)\right)^{-1},$$

$$A_r(1,1) = JA_r(0,0)\tau_r^r(1,0),$$
$$B^r(1,1) = B^r(1,0),$$
$$A_s(1,1) = A_s(1,0),$$
$$B^s(1,1) = B^s(1,0)[I - A_r(1,1)B^r(1,1)] = B^s(0,0)[I - A_r(1,1)B^r(1,0)].$$

The end effect of step 2 is to lower the norm of the lower left off-diagonal block:

$$\lambda_r^s(1,1) = \left[\frac{\mathrm{d}B^s(1,1)}{\mathrm{d}t} + B^s(1,1)J\right]A_r(1,1) = \mathrm{O}\left(\varepsilon\lambda_r^s(1,0)\right) = \mathrm{O}\left(\varepsilon\lambda_r^s(0,0)\right)$$

by an order $\varepsilon = |\tau_M/\tau_{M+1}| < 1$, thereby making the slow modes "purer" by decoupling them from the fast modes, while the upper right off-diagonal block is left unchanged:

$$\lambda_s^r(1,1) = \left[\frac{\mathrm{d}B^r(1,1)}{\mathrm{d}t} + B^r(1,1)J\right]A_s(1,1) = \left[\frac{\mathrm{d}B^r(1,0)}{\mathrm{d}t} + B^r(1,0)J\right]A_s(1,0) = \lambda_s^r(1,0) = \mathrm{O}\left(\varepsilon\lambda_s^r(0,0)\right).$$

As already pointed out, the refinement in Phase (1) is identical to one Mises Power method [38] for finding eigenvalues and eigenvectors of J. It follows that if the eigenvectors of J are chosen as initial basis in Eq. (23), Phase (1) is redundant.

3.2. Phase (2)

In the refinements of Phase (2) the basis vector time derivatives are calculated. As indicated above, including these terms in the refinements accounts for the high-order effects of nonlinearities, resulting in a better decoupling between fast and slow subspaces. The initial basis may be chosen as that resulting from Phase (1) or as the eigenvectors of J (in which case Phase (1) is skipped).

3.2.1. Step 1: the B^r-refinement

The B^r-refinement yields

$$\lambda_r^r(1,1) = \left(\frac{\mathrm{d}B^r(1,1)}{\mathrm{d}t} + B^r(1,1)J\right)A_r(1,1),$$
$$\tau_r^r(1,1) = \left(\lambda_r^r(1,1)\right)^{-1},$$

$$B^r(2,1) = \tau_r^r(1,1)\left[\frac{\mathrm{d}B^r(1,1)}{\mathrm{d}t} + B^r(1,1)J\right] = \tau_r^r(1,1)\left[\frac{\mathrm{d}B^r(1,0)}{\mathrm{d}t} + B^r(1,0)J\right],$$
$$A_r(2,1) = A_r(1,1),$$
$$B^s(2,1) = B^s(1,1),$$
$$A_s(2,1) = [I - A_r(2,1)B^r(2,1)]A_s(1,1) = [I - A_r(1,1)B^r(2,1)]A_s(1,0).$$

The effect of step 1 is to lower the norm of the upper-right off-diagonal block:

$$\lambda_s^r(2,1) = \left[\frac{\mathrm{d}B^r(2,1)}{\mathrm{d}t} + B^r(2,1)J\right]A_s(2,1) = \mathrm{O}\left(\varepsilon\lambda_s^r(1,1)\right) = \mathrm{O}\left(\varepsilon\lambda_s^r(1,0)\right) = \mathrm{O}\left(\varepsilon^2\lambda_s^r(0,0)\right)$$

by an order $\varepsilon = |\tau_M/\tau_{M+1}| < 1$, thereby making the fast modes "purer" by decoupling them from the slow modes, while the lower left off-diagonal block is left unchanged:

$$\lambda_r^s(2,1) = \left[\frac{\mathrm{d}B^s(2,1)}{\mathrm{d}t} + B^s(2,1)J\right]A_r(2,1) = \left[\frac{\mathrm{d}B^s(1,1)}{\mathrm{d}t} + B^s(1,1)J\right]A_r(1,1)$$
$$= \lambda_r^s(1,1) = \mathrm{O}\left(\varepsilon\lambda_r^s(1,0)\right) = \mathrm{O}\left(\varepsilon\lambda_r^s(0,0)\right).$$

3.2.2. Step 2: the A_r-refinement

The A_r-refinement yields

$$\lambda_r^r(2,1) = \left(\frac{\mathrm{d}B^r(2,1)}{\mathrm{d}t} + B^r(2,1)J\right)A_r(2,1),$$
$$\tau_r^r(2,1) = \left(\lambda_r^r(2,1)\right)^{-1},$$
$$A_r(2,2) = \left[-\frac{\mathrm{d}A_r(2,1)}{\mathrm{d}t} + JA_r(2,1)\right]\tau_r^r(2,1) = \left[-\frac{\mathrm{d}A_r(1,1)}{\mathrm{d}t} + JA_r(1,1)\right]\tau_r^r(2,1),$$
$$B^r(2,2) = B^r(2,1),$$
$$A_s(2,2) = A_s(2,1),$$
$$B^s(2,2) = B^s(2,1)[I - A_r(2,2)B^r(2,2)] = B^s(1,1)[I - A_r(2,2)B^r(2,1)].$$

The effect of step 2 is to lower the norm of the lower-left off-diagonal block:

$$\lambda_r^s(2,2) = \left[\frac{\mathrm{d}B^s(2,2)}{\mathrm{d}t} + B^s(2,2)J\right]A_r(2,2) = \mathrm{O}\left(\varepsilon\lambda_r^s(2,1)\right) = \mathrm{O}\left(\varepsilon^2\lambda_r^s(1,0)\right) = \mathrm{O}\left(\varepsilon^2\lambda_r^s(0,0)\right)$$

by an order $\varepsilon = |\tau_M/\tau_{M+1}| < 1$, thereby making the slow modes "purer" by decoupling them from the fast modes, while the upper right off-diagonal block is left unchanged:

$$\lambda_s^r(2,2) = \left[\frac{\mathrm{d}B^r(2,2)}{\mathrm{d}t} + B^r(2,2)J\right]A_s(2,2) = \left[\frac{\mathrm{d}B^r(2,1)}{\mathrm{d}t} + B^r(2,1)J\right]A_s(2,1)$$
$$= \lambda_s^r(2,1) = \mathrm{O}\left(\varepsilon\lambda_s^r(1,1)\right) = \mathrm{O}\left(\varepsilon\lambda_s^r(1,0)\right) = \mathrm{O}\left(\varepsilon^2\lambda_s^r(0,0)\right).$$

4. Time rates of change of CSP vectors

To actually carry out the calculations involved in Phase (2) requires computing a number of time derivatives of the CSP vectors. The derivation yielding the formulae to evaluate these terms is reported in Appendix B. For convenience, the main results are summarized below:

$$\frac{\mathrm{d}B^r(1,1)}{\mathrm{d}t} = \frac{\mathrm{d}B^r(1,0)}{\mathrm{d}t} = \tau_r^r(0,0)B^r(0,0)\frac{\mathrm{d}J}{\mathrm{d}t}[I - A_r(0,0)B^r(1,0)], \tag{24}$$

$$\frac{\mathrm{d}A_r(2,1)}{\mathrm{d}t} = \frac{\mathrm{d}A_r(1,1)}{\mathrm{d}t} = [I - A_r(1,1)B^r(1,0)]\frac{\mathrm{d}J}{\mathrm{d}t}A_r(0,0)\tau_r^r(1,0) - A_r(1,1)\frac{\mathrm{d}B^r(1,0)}{\mathrm{d}t}A_r(1,1), \tag{25}$$

$$\begin{aligned}\frac{\mathrm{d}B^r(2,1)}{\mathrm{d}t} = {} & \tau_r^r(1,1)\left[\frac{\mathrm{d}B^r(1,0)}{\mathrm{d}t}J + B^r(1,0)\frac{\mathrm{d}J}{\mathrm{d}t} + \frac{\mathrm{d}^2B^r(1,0)}{\mathrm{d}t^2}\right][I - A_r(1,1)B^r(2,1)] \\ & - B^r(2,1)\frac{\mathrm{d}A_r(1,1)}{\mathrm{d}t}B^r(2,1),\end{aligned} \tag{26}$$

where

$$\begin{aligned}\frac{\mathrm{d}^2B^r(1,0)}{\mathrm{d}t^2} = {} & \left[\frac{\mathrm{d}\tau_r^r(0,0)}{\mathrm{d}t}B^r(0,0)\frac{\mathrm{d}J}{\mathrm{d}t} + \tau_r^r(0,0)B^r(0,0)\frac{\mathrm{d}^2J}{\mathrm{d}t^2}\right][I - A_r(0,0)B^r(1,0)] \\ & - \tau_r^r(0,0)B^r(0,0)\frac{\mathrm{d}J}{\mathrm{d}t}A_r(0,0)\frac{\mathrm{d}B^r(1,0)}{\mathrm{d}t}.\end{aligned} \tag{27}$$

Since Eq. (27) involves the evaluation of the time rate of change of the Jacobian matrix $\mathrm{d}J/\mathrm{d}t$, and of higher-order rates $\mathrm{d}^2J/\mathrm{d}t^2$ as well, and given that Eqs. (24)–(26) involve $\mathrm{d}J/\mathrm{d}t$, it follows that, in Phase (2), the B^r-refinement requires the availability of $\mathrm{d}J/\mathrm{d}t$, while the A_r-refinement requires the availability of both $\mathrm{d}J/\mathrm{d}t$ and $\mathrm{d}^2J/\mathrm{d}t^2$. These quantities can be evaluated from the expressions:

$$\frac{\mathrm{d}J}{\mathrm{d}t} = \sum_{i=1,N_s}\frac{\partial J}{\partial y^i}\frac{\mathrm{d}y^i}{\mathrm{d}t} = \sum_{i=1,N_s}\frac{\partial J}{\partial y^i}g^i, \tag{28}$$

$$\frac{\mathrm{d}^2J}{\mathrm{d}t^2} = \sum_{i,j=1,N_s}\left[\frac{\partial^2 J}{\partial y^i\partial y^j}g^i + \frac{\partial J}{\partial y^i}J\right]g^j, \tag{29}$$

which show that $\mathrm{d}J/\mathrm{d}t$ and $\mathrm{d}^2J/\mathrm{d}t^2$ depend on the state of the system only. They are local measures of the geometrical characteristics of the manifold (such as local curvature and higher-order terms), since they involve the terms $\partial J/\partial y^i$ and $\partial^2 J/\partial y^i\partial y^j$. As a consequence, the time rates of change of the CSP vectors also depend exclusively on the local state variables. Hence, tabulation methods, such as PRISM [32] or ISAT [33], can also be used with the CSP refinement procedure to generate look-up tables, either on-line or off-line, for SIMs of high-order accuracy found by means of the CSP refinements procedure.

5. The Davis–Skodje problem

The model problem analyzed in this section and the next was first proposed by Davis and Skodje in [14]. It allows us to demonstrate the ability of CSP iterations to return the correct asymptotic expansion of the approximate SIM for a stiff system with an explicit, constant, small parameter and prescribed slow and fast variables. This same goal has been pursued by Zagaris et al. in [23] with reference to the Michaelis and Menten mechanism. Since this model is planar ($N = 2$), it is possible to evaluate the CSP vectors and their time rates of change algebraically.

Consider then the following system of ODEs:

$$\frac{\mathrm{d}y}{\partial t} = \frac{1}{\varepsilon}\left(-y + \frac{z}{1+z}\right) - \frac{z}{(1+z)^2}, \tag{30}$$

$$\frac{\mathrm{d}z}{\partial t} = -z, \tag{31}$$

subject to the initial conditions $y(0) = y_0$ and $z(0) = z_0$; the small parameter ε is explicit and constant and much smaller than one, and the prescribed slow and fast variables are z and y, respectively. This system has the analytical solution:

$$y(t) = \left(y_0 - \frac{z_0}{1+z_0}\right)e^{-t/\varepsilon} + \frac{z_0 e^{-t}}{1+z_0 e^{-t}}, \tag{32}$$

$$z(t) = z_0 e^{-t}. \tag{33}$$

Given an arbitrary initial condition (y_0, z_0), off the manifold, $y(t)$ first experiences a fast rate of change in the initial $O(\varepsilon)$ time period, followed by a slow rate of change at later times. As shown in Fig. 1, the solution trajectory, for times $t \gg \varepsilon$, closely follows the slow manifold defined by the equation:

$$h_\varepsilon(y,z) = y - \frac{z}{1+z} = 0, \tag{34}$$

which is invariant under the dynamics of Eqs. (30) and (31) for $z \geqslant 0$, and is independent of ε [14,13].

5.1. The optimal CSP vectors

Let us now examine what one would expect to achieve after employing the CSP method. According to CSP, Eqs. (30) and (31) can be recast in the form:

$$\frac{d}{dt}\begin{bmatrix} y \\ z \end{bmatrix} = \boldsymbol{a}_1 f^1 + \boldsymbol{a}_2 f^2. \tag{35}$$

Since, according to the differential equations (30) and (31) and the solutions (32) and (33), the fast time scale affects only the variable y, the fast movement of the solution towards the manifold is expected to take place

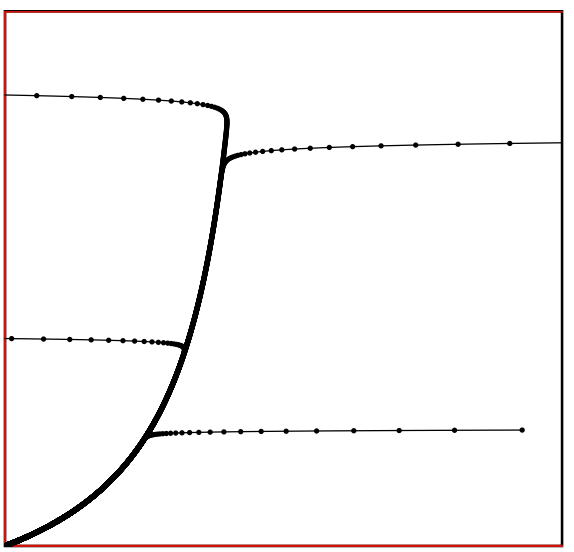

along the y-axis. It is reasonable then for the vector $\boldsymbol{a}_1$, along which the fast time scale acts, to have the form:

$$\boldsymbol{a}_1 = [1, 0]^{\mathrm{T}}. \tag{36}$$

Indeed, as shown in Fig. 1, during the initial fast transient period, the fast time scale tends to move the solution along a trajectory parallel to the y-axis towards the manifold, independent of the initial values y_0 and z_0. In addition, knowing the expression describing the manifold, Eq. (34), in order for the amplitude f^1 to vanish as soon as the trajectory hits the manifold, the $\boldsymbol{b}^1$ vector must be given by

$$\boldsymbol{b}^1 = [1, -(1+z)^{-2}] \tag{37}$$

so that when the fast time scale has been exhausted, i.e. $t \gg \varepsilon$, the fast amplitude:

$$f^1 = \boldsymbol{b}^1 \cdot \boldsymbol{g} = (1)\left[\frac{1}{\varepsilon}\left(-y + \frac{z}{1+z}\right) - \frac{z}{(1+z)^2}\right] + \left(\frac{-1}{(1+z)^2}\right)[-z] = \frac{1}{\varepsilon}\left(-y + \frac{z}{1+z}\right) \tag{38}$$

becomes exponentially small and the first mode in Eq. (35) can be neglected. Furthermore, differentiating Eq. (34) shows that when the fast time scale has been exhausted and the solution moves slowly on the manifold, we have

$$\mathrm{d}y = \frac{1}{(1+z)^2}\mathrm{d}z \tag{39}$$

suggesting that the vector $\boldsymbol{a}_2$ has the form:

$$\boldsymbol{a}_2 = [(1+z)^{-2}, 1]^{\mathrm{T}}. \tag{40}$$

Finally, since the amplitude f^2 is desired to vary at all times slowly, a reasonable choice for the vector $\boldsymbol{b}^2$ is

$$\boldsymbol{b}^2 = [0, 1] \tag{41}$$

so that

$$f^2 = \boldsymbol{b}^2 \cdot \boldsymbol{g} = (0)\left[\frac{1}{\varepsilon}\left(-y + \frac{z}{1+z}\right) - \frac{z}{(1+z)^2}\right] + (1)[-z] = -z. \tag{42}$$

The basis vectors Eqs. (36) and (40), (37) and (41) are linearly independent and orthogonal. They further provide

$$\Lambda_1^1 = -\frac{1}{\varepsilon}, \quad \Lambda_2^1 = 0, \tag{43}$$

$$\Lambda_1^2 = 0, \qquad \Lambda_2^2 = -1, \tag{44}$$

indicating that the fast and slow amplitudes, f^1 and f^2, are indeed fully decoupled from each other. In summary, the CSP form, Eq. (35), of the governing equations (30) and (31) is

$$\frac{\mathrm{d}}{\mathrm{d}t}\begin{bmatrix} y \\ z \end{bmatrix} = \begin{bmatrix} 1 \\ 0 \end{bmatrix} f^1 + \begin{bmatrix} (1+z)^{-2} \\ 1 \end{bmatrix} f^2, \tag{45}$$

where, using the solutions (32) and (33),

$$\begin{aligned} f^1 &= \frac{-1}{\varepsilon}\left(y_0 - \frac{z_0}{1+z_0}\right)\mathrm{e}^{-t/\varepsilon}, \\ f^2 &= -z_0\mathrm{e}^{-t}. \end{aligned} \tag{46}$$

It follows that, when the fast time scale becomes exhausted, i.e. $t \gg \varepsilon$, the amplitude f^1 becomes sufficiently small and the governing equations simplify to

$$\frac{\mathrm{d}}{\mathrm{d}t}\begin{bmatrix} y \\ z \end{bmatrix} \approx \begin{bmatrix} (1+z)^{-2} \\ 1 \end{bmatrix}(-z) \tag{47}$$

accompanied by the algebraic relation $f^1 \approx 0$, which describes the manifold. Clearly, the simplified problem Eq. (47) is non-stiff and its solution is given by

$$\begin{aligned} y_s(t) &= \frac{z_0 \mathrm{e}^{-t}}{1+z_0\mathrm{e}^{-t}} - \varepsilon f_*^1, \\ z_s(t) &= z_0 \mathrm{e}^{-t}, \end{aligned} \tag{48}$$

where

$$f_*^1 = \frac{1}{\varepsilon}\left(-y_* + \frac{z_*}{1+z_*}\right) = \frac{1}{\varepsilon}\left(-y_0 + \frac{z_0}{1+z_0}\right)\mathrm{e}^{-\tau_*/\varepsilon}.$$

The symbol τ_* denotes the time at which the solution starts to be computed from the simplified set of Eq. (47) and y_* and z_* are the values of the variables y and z at $t = \tau_*$. Regarding the fast variable y, the relative error between the solution obtained from the full and the simplified problem for $t > \tau_*$ is given by the expression:

$$y(t) - y_s(t) = \left(y_0 - \frac{z_0}{1+z_0}\right)\mathrm{e}^{-\tau_*/\varepsilon}\left(\mathrm{e}^{t/\tau_*} - 1\right) \tag{49}$$

demonstrating the accuracy achieved by the particular basis vectors used and the resulting simplified problem.

The identification of optimal basis vectors allowing the construction of the exact SIM and of the related simplified non-stiff problem cannot be performed so easily when the problem is more complex.[2] In that case, the iterative procedure presented earlier must be employed. Let us now describe what this iterative procedure provides for the simple problem examined here.

5.2. An arbitrary initial set of basis vectors

Suppose that the initial guess[3] for the basis vectors, i.e. $(k, m) = (0, 0)$, is

$$\begin{aligned} &\boldsymbol{a}_1(0,\,0) = \begin{bmatrix} 1 \\ 1 \end{bmatrix}, \quad \boldsymbol{a}_2(0,\,0) = \begin{bmatrix} 0 \\ -1 \end{bmatrix}, \\ &\boldsymbol{b}^1(0,\,0) = [1, 0], \quad \boldsymbol{b}^2(0,\,0) = [1, -1] \end{aligned} \tag{50}$$

so that

[2] It can be shown however that the optimal basis vectors coincide with the eigenvectors of the linear propagator, also referred to as monodromy, matrix of the dynamical system [39,40].

[3] As initial basis, we could have chosen the identity matrix. However, for the Davis–Skodje problem, this choice provides directly $\Lambda_1^2 = 0$ after the first A_r-refinement. This would prevent us from demonstrating the effect on the A_r-refinements under general circumstances.

$$f^1(0,0) = \frac{1}{\varepsilon}\left(-y + \frac{z}{1+z}\right) - \frac{z}{(1+z)^2}, \tag{51}$$

$$f^2(0,0) = \frac{1}{\varepsilon}\left(-y + \frac{z}{1+z}\right) - \frac{z}{(1+z)^2} + z, \tag{52}$$

and

$$\Lambda_1^1(0,\,0) = -\frac{1}{\varepsilon}\Psi, \quad \Lambda_2^1(0,\,0) = -\frac{1}{\varepsilon}F_z, \tag{53}$$

$$\Lambda_1^2(0,\,0) = -\frac{1}{\varepsilon}\Psi + 1, \quad \Lambda_2^2(0,\,0) = -\frac{1}{\varepsilon}F_z - 1, \tag{54}$$

where

$$F_z = \frac{1}{(1+z)^2} - \varepsilon\frac{1-z}{(1+z)^3}$$

and $\Psi = 1 - F_z$.

Obviously, when the fast time scale becomes exhausted, the fast amplitude is not negligible, but $f^1(0, 0) = O(1)$. In addition, the reduced system

$$\frac{\mathrm{d}}{\mathrm{d}t}\begin{bmatrix} y \\ z \end{bmatrix} \approx \begin{bmatrix} 0 \\ -1 \end{bmatrix}\left(\frac{1}{\varepsilon}\left(-y + \frac{z}{1+z}\right) - \frac{z}{(1+z)^2} + z\right) \tag{55}$$

is stiff and produces an O(1) error. These results are related to the fact that, as Eqs. (53) and (54) show, all Λ_j^i are $O(\varepsilon^{-1})$.

5.3. The role of B^r-refinements

Performing one B^r-refinement, i.e. $(k, m) = (1, 0)$, as illustrated in Section 2, where the time derivatives of the basis vectors are evaluated analytically, Eqs. (21) and (22), yields

$$\boldsymbol{a}_1(1,0) = \Psi\begin{bmatrix} 1 \\ 1 \end{bmatrix}, \quad \boldsymbol{a}_2(1,0) = -(\Psi)^{-1}\begin{bmatrix} F_z \\ 1 \end{bmatrix},$$

$$\boldsymbol{b}^1(1,0) = [1, -F_z], \quad \boldsymbol{b}^2(1,0) = [1, -1], \tag{56}$$

and

$$f^1(1,0) = \frac{1}{\varepsilon}\left(-y + \frac{z}{1+z}\right) - \frac{\varepsilon z(1-z)}{(1+z)^3}, \tag{57}$$

$$f^2(1,0) = \frac{1}{\varepsilon}\left(-y + \frac{z}{1+z}\right) - \frac{z}{(1+z)^2} + z, \tag{58}$$

and

$$\Lambda_1^1(1,0) = -\frac{1}{\varepsilon}\left[1 - \frac{\varepsilon F_z}{\Psi}\right], \quad \Lambda_2^1(1,0) = -\frac{F_z - G_z}{\Psi^2}, \tag{59}$$

$$\Lambda_1^2(1,0) = 1 - \frac{\Psi}{\varepsilon}, \quad \Lambda_2^2(1,0) = -\frac{1}{\Psi}. \tag{60}$$

Relative to the $(k, m) = (0, 0)$ case, it is seen that by making one B^r-refinement the accuracy in the description of the manifold is improved by one order in ε, since after the fast transient, i.e. for $t \gg \varepsilon$,

$f^1(1,0) = O(\varepsilon^1)$ while $f^1(0,0) = O(\varepsilon^0)$. According to Eq. (59), this is a direct result of the change in magnitude of Λ_2^1, which goes from $\Lambda_2^1(0,0) = O(\varepsilon^{-1})$ to $\Lambda_2^1(1,0) = O(\varepsilon^0)$. As expected, the value of Λ_1^2 does not change, $\Lambda_1^2(0,0) = \Lambda_1^2(1,0) = O(\varepsilon^{-1})$, leaving the coupling of the slow amplitude f^2 to the fast one f^1 unaltered. Furthermore, the values of Λ_1^1 and Λ_2^2 tend to their optimal values. As a result, the reduced system

$$\frac{\mathrm{d}}{\mathrm{d}t}\begin{bmatrix} y \\ z \end{bmatrix} \approx -\Psi^{-1}\begin{bmatrix} F_z \\ 1 \end{bmatrix}\left(\frac{1}{\varepsilon}\left(-y + \frac{z}{1+z}\right) - \frac{z}{(1+z)^2} + z\right) \tag{61}$$

is still stiff but now produces an $O(\varepsilon^1)$ error in the $t \gg \varepsilon$ period. Performing further B^r-refinements, yields the results collected in Table 1, i.e. the optimal CSP expressions are recovered for $\boldsymbol{b}^1$, Λ_1^1, Λ_2^1 and Λ_2^2. In contrast, $\boldsymbol{a}_1$, $\boldsymbol{b}^2$ and Λ_1^2 remain as guessed initially.

5.4. The role of A_r-refinements

Returning to the initial guess for the basis vectors (50), one A^r-refinement $(k, m) = (0, 1)$, as illustrated in Section 2, where the time derivatives of the basis vectors are evaluated analytically, Eqs. (21) and (22), yields

$$\begin{aligned} \boldsymbol{a}_1(0,1) &= \begin{bmatrix} 1 \\ \varepsilon\Psi^{-1} \end{bmatrix}, \quad \boldsymbol{a}_2(0,1) = \begin{bmatrix} 0 \\ 1 \end{bmatrix}, \\ \boldsymbol{b}^1(0,1) &= [1,0], \quad \boldsymbol{b}^2(0,1) = [-\varepsilon\Psi^{-1}, 1], \end{aligned} \tag{62}$$

and

$$f^1(0,1) = \frac{1}{\varepsilon}\left(-y + \frac{z}{1+z}\right) - \frac{z}{(1+z)^2}, \tag{63}$$

$$f^2(0,1) = \frac{1}{\Psi}\left[\left(-y + \frac{z}{1+z}\right) - \frac{\varepsilon z}{(1+z)^2}\right] - z, \tag{64}$$

and

$$\Lambda_1^1(0,1) = -\frac{1}{\varepsilon}\left[1 - \frac{\varepsilon F_z}{\Psi}\right], \quad \Lambda_2^1(0,1) = \frac{1}{\varepsilon}F_z, \tag{65}$$

$$\Lambda_1^2(0,1) = \frac{1}{\Psi} - \varepsilon\frac{1+G_z}{\Psi^2}, \quad \Lambda_2^2(0,1) = -\frac{1}{\Psi}, \tag{66}$$

where

$$G_z = \frac{(2-\varepsilon)z}{(1+z)^3} - \varepsilon\frac{3z(1-z)}{(1+z)^4}.$$

Table 1
The role of B^r-refinements

(k, m)	$\boldsymbol{b}^1$	Λ_1^1	Λ_2^2	Λ_2^1
(0, 0)	[1, 0]	$-\frac{1}{\varepsilon} + O(1/\varepsilon)$	$-1 + O(1/\varepsilon)$	$O(1/\varepsilon)$
(1, 0)	$[1, -\frac{1}{(1+z)^2} + O(1)]$	$-\frac{1}{\varepsilon} + O(1)$	$-1 + O(1)$	$O(1)$
(2, 0)	$[1, -\frac{1}{(1+z)^2} + O(\varepsilon)]$	$-\frac{1}{\varepsilon} + O(\varepsilon)$	$-1 + O(\varepsilon)$	$O(\varepsilon)$
⋮	⋮	⋮	⋮	⋮
$(\infty, 0)$	$[1, -\frac{1}{(1+z)^2}]$	$-\frac{1}{\varepsilon}$	-1	0

Relative to the $(k, m) = (0, 0)$ case, it is seen that, by making one A_r-refinement, the accuracy in the description of the manifold is not improved, since $\boldsymbol{b}^1(0, 1) = \boldsymbol{b}^1(0, 0)$ and, therefore, $f^1(0, 1) = f^1(0, 0) = \mathrm{O}(1)$ at $t \gg \varepsilon$. What changes is the magnitude of Λ_1^2 and Λ_2^2 which, from $\Lambda_1^2(0, 0) = \mathrm{O}(\varepsilon^{-1})$ and $\Lambda_2^2(0, 0) = \mathrm{O}(\varepsilon^{-1})$, now become $\Lambda_1^2(0, 1) = \mathrm{O}(\varepsilon^0)$ and $\Lambda_2^2(0, 1) = -1 + \mathrm{O}(\varepsilon^0)$ converging to their optimal values. Due to these developments, the reduced system

$$\frac{\mathrm{d}}{\mathrm{d}t}\begin{bmatrix} y \\ z \end{bmatrix} \approx \begin{bmatrix} 0 \\ 1 \end{bmatrix}\left(\frac{1}{\Psi}\left[\left(-y + \frac{z}{1+z}\right) - \frac{\varepsilon z}{(1+z)^2}\right] - z\right) \tag{67}$$

is now non-stiff but still produces an O(1) error. Performing further A_r-refinements, yields the results collected in Table 2, i.e. the optimal CSP expressions are recovered for $\boldsymbol{a}_1$, Λ_1^1, Λ_1^2 and Λ_2^2. In contrast, $\boldsymbol{b}^1$, $\boldsymbol{a}_2$ and Λ_2^1 remain as guessed initially.

5.5. Combining the action of A_r- and B^r-refinements

Starting with the initial guess for the basis vectors (50) and performing first one A_r-refinement and then one B^r-refinement $(k, m) = (1, 1)$, as illustrated in Section 2, where the time derivatives of the basis vectors are evaluated analytically, yields

$$\boldsymbol{a}_1(1, 1) = \begin{bmatrix} 1 \\ \varepsilon\Psi^{-1} \end{bmatrix}, \quad \boldsymbol{a}_2(1, 1) = \begin{bmatrix} -\Psi \\ \overline{1 - (1+\varepsilon)F_z} \end{bmatrix}\begin{bmatrix} F_z \\ 1 \end{bmatrix}, \tag{68}$$

$$\boldsymbol{b}^1(1, 1) = \left[\frac{\Psi}{1 - (1+\varepsilon)F_z}\right][1, -F_z], \quad \boldsymbol{b}^2(1, 1) = [\varepsilon\Psi^{-1}, -1], \tag{69}$$

and

$$f^1(1, 1) = \left[\frac{1}{\varepsilon}\left(-y + \frac{z}{1+z}\right) - \varepsilon\frac{z(1-z)}{(1+z)^3}\right]\left[\frac{\Psi}{1 - (1+\varepsilon)F_z}\right], \tag{70}$$

$$f^2(1, 1) = \left[\left(-y + \frac{z}{1+z}\right) - \frac{\varepsilon}{(1+z)^2} + z\Psi\right]\left[\frac{1}{\Psi}\right], \tag{71}$$

$$\Lambda_1^1(1, 1) = -\frac{1}{\varepsilon} + \mathrm{O}(\varepsilon^1), \quad \Lambda_2^1(1, 1) = \mathrm{O}(\varepsilon^0), \tag{72}$$

$$\Lambda_1^2(1, 1) = \mathrm{O}(\varepsilon^0), \quad \Lambda_2^2(1, 1) = -1 + \mathrm{O}(\varepsilon^1). \tag{73}$$

It is seen that, in comparison to the $(k, m) = (0, 0)$ case, the fast amplitude decays to a lower value when the fast time scale becomes exhausted, i.e. $t \gg \varepsilon$, i.e. $f^1(1, 1) = \mathrm{O}(\varepsilon^1)$ from $f^1(0, 0) = \mathrm{O}(\varepsilon^0)$, thus improving the accuracy of the description of the manifold and the accuracy of the solution provided by the simplified problem. It is easy to show that this is due to the fact that the magnitude of Λ_2^1 decreases by an order, i.e. from $\Lambda_2^1(0, 0) = \mathrm{O}(\varepsilon^{-1})$ to $\Lambda_2^1(1, 1) = \mathrm{O}(\varepsilon^0)$. Furthermore, the simplified system

Table 2
The role of A_r-refinements

(k, m)	$\boldsymbol{a}_1$	Λ_1^1	Λ_2^2	Λ_1^2
(0, 0)	$[1, 1]^{\mathrm{T}}$	$-\frac{1}{\varepsilon} + \mathrm{O}(1/\varepsilon)$	$-1 + \mathrm{O}(1/\varepsilon)$	$\mathrm{O}(1/\varepsilon)$
(0, 1)	$[1, \mathrm{O}(\varepsilon)]^{\mathrm{T}}$	$-\frac{1}{\varepsilon} + \mathrm{O}(1)$	$-1 + \mathrm{O}(1)$	$\mathrm{O}(1)$
(0, 2)	$[1, \mathrm{O}(\varepsilon^2)]^{\mathrm{T}}$	$-\frac{1}{\varepsilon} + \mathrm{O}(\varepsilon)$	$-1 + \mathrm{O}(\varepsilon)$	$\mathrm{O}(\varepsilon)$
⋮	⋮	⋮	⋮	⋮
$(0, \infty)$	$[1, 0]^{\mathrm{T}}$	$-\frac{1}{\varepsilon}$	-1	0

$$\frac{\mathrm{d}}{\mathrm{d}t}\begin{bmatrix} y \\ z \end{bmatrix} \approx \begin{bmatrix} F_z \\ 1 \end{bmatrix}\left(\left(-y+\frac{z}{1+z}\right)-\frac{\varepsilon}{(1+z)^2}-z\Psi\right)\left(\frac{1}{\Psi+\varepsilon F_z}\right) \tag{74}$$

is now non-stiff since the magnitude of Λ_1^2 decreases by an order; i.e. from $\Lambda_1^2(0,\,0)=\mathrm{O}(\varepsilon^{-1})$ to $\Lambda_1^2(1,1)=\mathrm{O}(\varepsilon^0)$. Finally, the diagonal elements Λ_1^1 and Λ_2^2 converge to their optimal values, i.e. from $\Lambda_1^1(0,\,0)=-\varepsilon^{-1}+O(\varepsilon^{-1})$ and $\Lambda_2^2(0,\,0)=-1+O(\varepsilon^{-1})$ to $\Lambda_1^1(1,1)=-\varepsilon^{-1}+O(\varepsilon^0)$ and $\Lambda_2^2(1,1)=-1+O(\varepsilon^0)$.

5.6. The eigenvectors as the initial set of basis vectors

Similar results, regarding the accuracy of the description of the manifold and the accuracy and non-stiffness of the simplified problem, provided by one B^r and one A_r refinements, $(k, m) = (1, 1)$, are also obtained if the eigenvectors of the 2×2 Jacobian of the RHS in Eqs. (30) and (31) are used as CSP vectors:

$$\begin{aligned} \boldsymbol{a}_1 &= \begin{bmatrix} 1 \\ 0 \end{bmatrix}, \quad \boldsymbol{a}_2 = \begin{bmatrix} \frac{F_z}{1-\varepsilon} \\ 1 \end{bmatrix}, \\ \boldsymbol{b}^1 &= \left[1, \frac{-F_z}{1-\varepsilon}\right], \quad \boldsymbol{b}^2 = [0,1]. \end{aligned} \tag{75}$$

Such a choice yields

$$\begin{aligned} f^1 &= \frac{1}{\varepsilon}\left(-y+\frac{z}{1+z}\right)+\frac{\varepsilon}{1-\varepsilon}\frac{2z^2}{(1+z)^3}, \\ f^2 &= -z \end{aligned} \tag{76}$$

with

$$\Lambda_1^1=\lambda(1)=-\frac{1}{\varepsilon}, \quad \Lambda_2^1=\frac{-G_z}{1-\varepsilon}, \tag{77}$$

$$\Lambda_1^2=0, \quad \Lambda_2^2=\lambda(2)=-1. \tag{78}$$

As with the $(k, m) = (1, 1)$ case, it is seen that $f^1 = \mathrm{O}(\varepsilon)$ when the fast time scale becomes exhausted, i.e. $t \gg \varepsilon$. Again, such a decrease is allowed by the values $\Lambda_1^1 = \mathrm{O}(\varepsilon^{-1})$ and $\Lambda_2^1 = \mathrm{O}(\varepsilon^0)$. Furthermore, the values of Λ_1^2 and Λ_2^2 produce the reduced problem:

$$\frac{\mathrm{d}}{\mathrm{d}t}\begin{bmatrix} y \\ z \end{bmatrix} \approx \begin{bmatrix} \frac{F_z}{1-\varepsilon} \\ 1 \end{bmatrix}(-z) \tag{79}$$

which is non-stiff and, since $f^1 = \mathrm{O}(\varepsilon)$, produces an $\mathrm{O}(\varepsilon)$ error.

5.7. Impact of time derivatives of CSP vectors on manifold accuracy

Let us examine in detail the effects of the time derivatives of the CSP vectors, involved in the B^r-refinement, on the accuracy of the SIM. Let us start from the following choice of basis vectors:

$$\begin{aligned} \boldsymbol{a}_1(0,\,0) &= \begin{bmatrix} 1 \\ 0 \end{bmatrix}, \quad \boldsymbol{b}^1(0,\,0) = [1,0], \\ \boldsymbol{a}_2(0,\,0) &= \begin{bmatrix} 0 \\ 1 \end{bmatrix}, \quad \boldsymbol{b}^2(0,\,0) = [0,1]. \end{aligned} \tag{80}$$

Let us consider separately the two cases of (i) neglecting or (ii) including the time derivative terms during the B^r-refinements. If the time derivative terms are neglected, one finds with increasing number of B^r-refinements for the first (fast) basis vector, and corresponding amplitude, the results listed in Tables 3 and 4, respectively.

The $\boldsymbol{b}^1$ vector converges to the "fast" left eigenvector; $f^1(k, 0)$ decays to $O(\varepsilon^1)$ when the fast time scale is exhausted, and the manifold, defined by the equation $f^1(k, 0) = 0$, is obtained with an $O(\varepsilon^{1+1})$ accuracy as shown in Fig. 2 [Left]. This clearly shows that neglecting the contribution of the nonlinearities, as represented by the time derivatives of the basis vectors, hinders the possibility of improving the decoupling between the fast and slow subspace, and, in turn, improving the accuracy of the manifold description, which is always affected by an order $O(\varepsilon^{1+1})$ error, independent of the number of refinements.

If the time derivative terms are included, one finds with increasing number of B^r-refinements for the first (fast) basis vector, and corresponding amplitude, the results collected in Tables 5 and 6, respectively.

The $\boldsymbol{b}^1$ vector converges to the fast CSP vector identified by Eq. (37), $f^1(k, 0)$ decays to $O(\varepsilon^k)$ when the fast time scale is exhausted and the manifold is obtained with an $O(\varepsilon^{k+1})$ accuracy as shown in Fig. 2 [Right].

It is also worth noticing that the $O(\varepsilon)$ improvement in the accuracy of the amplitude of the first mode provided by the CSP refinements when $d\boldsymbol{b}/dt$ are included is obtained by a uniform improvement of the accuracy of each coefficient in the expansion of the manifold in powers of z, as shown in Table 7.

This finding illustrates how the B^r-refinements are able to generate, term by term, the asymptotic expression of the SIM. Such a result can also be obtained by the Fraser and Roussel method, at the expense of a higher computational cost and a less stable numerical procedure [14].

The ability of CSP iterations to return the correct asymptotic expansion of the approximate slow manifold was proven recently in [23] for a stiff system with reference to the Michaelis and Menten model characterized by having an explicit small parameter and prescribed slow and fast variables.

Table 3
Case (i): time derivatives are not included and $B^r(0, 0) = I$

(k, m)	$\boldsymbol{b}^1$	Λ_1^1	Λ_2^2	Λ_2^1
$(0, 0)$	$[1, 0]$	$-\frac{1}{\varepsilon}$	-1	$-F_z/\varepsilon$
$(1, 0)$	$[1, -F_z]$	$-\frac{1}{\varepsilon}$	-1	F_z
$(2, 0)$	$[1, -(1+\varepsilon)F_z]$	$-\frac{1}{\varepsilon}$	-1	εF_z
$\vdots$	$\vdots$	$\vdots$	$\vdots$	$\vdots$
$(\infty, 0)$	$[1, -\frac{F_z}{1-\varepsilon}]$	$-\frac{1}{\varepsilon}$	-1	0

The table shows how the $\boldsymbol{b}$ vectors and the Λ matrix change with B^r-refinements.

Table 4
Case (i): time derivatives are not included and $B^r(0, 0) = I$

$f^1(k, m)$	$O(\varepsilon^{-1})$	$O(1)$	$O(\varepsilon)$	$O(\varepsilon^2)$	$O(\varepsilon^3)$
$f^1(0, 0)$	$\frac{1}{\varepsilon}(-y+\frac{z}{1+z})$	$-\frac{z}{(1+z)^2}$			
$f^1(1, 0)$	$\frac{1}{\varepsilon}(-y+\frac{z}{1+z})$		$+\varepsilon\frac{(z-1)z}{(1+z)^3}$		
$f^1(2, 0)$	$\frac{1}{\varepsilon}(-y+\frac{z}{1+z})$		$+\varepsilon\frac{2z^2}{(1+z)^3}$	$+\varepsilon^2\frac{(z-1)z}{(1+z)^3}$	
$\vdots$	$\vdots$	$\vdots$	$\vdots$	$\vdots$	$\vdots$
$f^1(\infty, 0)$	$\frac{1}{\varepsilon}(-y+\frac{z}{1+z})$		$+\varepsilon\frac{2z^2}{(1+z)^3}$	$+\varepsilon^2\frac{2z^2}{(1+z)^3}$	$+\varepsilon^3\frac{2z^2}{(1+z)^3}\ldots$
f^1_{Eige}	$\frac{1}{\varepsilon}(-y+\frac{z}{1+z})$		$+\varepsilon\frac{2z^2}{(1+z)^3}$	$+\varepsilon^2\frac{2z^2}{(1+z)^3}$	$+\varepsilon^3\frac{2z^2}{(1+z)^3}\ldots$

The table shows how the first mode amplitude f^1 changes with B^r-refinements.

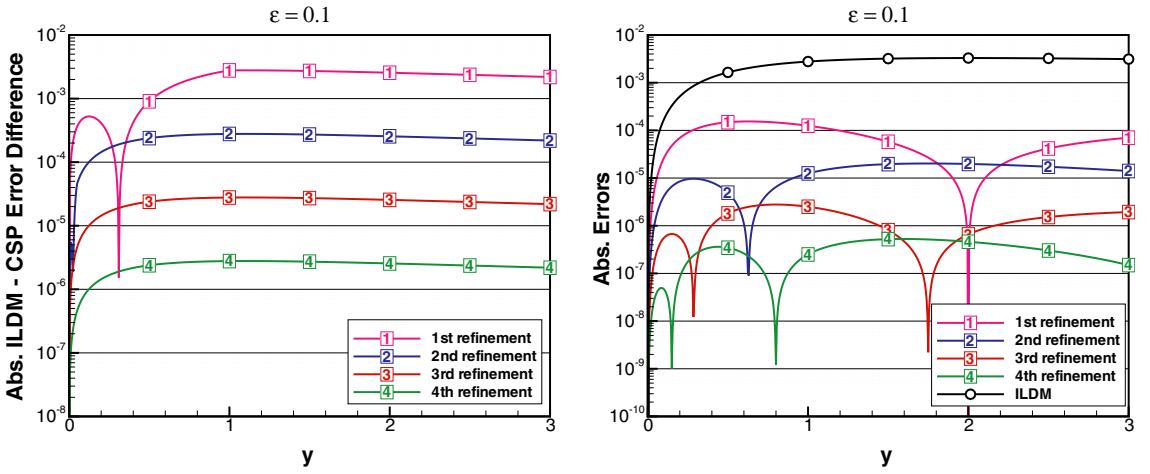

Fig. 2. [Left] CSP vectors converge to eigenvectors with CSP refinements when $d\boldsymbol{b}/dt$ are neglected; [Right] Manifold accuracy increases with CSP refinements when $d\boldsymbol{b}/dt$ are accounted for.

Table 5
Case (ii): time derivatives are included and $B^r(0, 0) = I$

(k, m)	$\boldsymbol{b}^1$	Λ_1^1	Λ_2^2	Λ_2^1
$(0, 0)$	$[1, 0]$	$-\frac{1}{\varepsilon}$	-1	$\frac{1+z-\varepsilon+z\varepsilon}{(1+z)^3\varepsilon}$
$(1, 0)$	$[1, -\frac{1}{(1+z)^2} + \varepsilon\frac{1-z}{(1+z)^3}]$	$-\frac{1}{\varepsilon}$	-1	$\frac{1+z-\varepsilon+z\varepsilon}{(1+z)^3}$
$(2, 0)$	$[1, -\frac{1}{(1+z)^2} + \varepsilon^2\frac{1-4z+z^2}{(1+z)^4}]$	$-\frac{1}{\varepsilon}$	-1	$-\varepsilon\frac{-1+\varepsilon-4z\varepsilon+z^2(1+\varepsilon)}{(1+z)^4}$
$\vdots$	$\vdots$	$\vdots$	$\vdots$	$\vdots$
$(\infty, 0)$	$[1, -\frac{1}{(1+z)^2}]$	$-\frac{1}{\varepsilon}$	-1	0

The table shows how the $\boldsymbol{b}^1$ vector and the Λ matrix change with B^r-refinements.

6. A 3-species kinetics problem

In this section, we introduce a model problem with the relevant features of a stiff chemical kinetics mechanism; this model is characterized by having a non-constant, non-explicitly defined, small parameter and non-prescribed slow and fast variables. Moreover, the CSP vectors and their time rates of change are sufficiently simple that they can still be evaluated algebraically, but complicated enough so as to allow a non-trivial validation of the procedures for the CSP refinements illustrated in Sections 4 and 5.

To this aim, let us consider the following set of three symbolic reactions modelling the dynamics of 3 species X, Y and Z:

$$\begin{aligned} X &= 2Y, \\ X + Y &= Z, \\ Y + Z &= X. \end{aligned} \tag{81}$$

Let also assume that the forward k^f and reverse k^b reaction rate constants of these three reactions are defined as

Table 6
Case (ii): time derivatives are included and $B^r(0,0) = I$

$f^1(k,m)$	$O(\varepsilon^{-1})$	$O(1)$	$O(\varepsilon)$	$O(\varepsilon^2)$	$O(\varepsilon^3)$
$f^1(0,0)$	$\frac{1}{\varepsilon}(-y+\frac{z}{1+z})$	$-\frac{z}{(1+z)^2}$			
$f^1(1,0)$	$\frac{1}{\varepsilon}(-y+\frac{z}{1+z})$		$+\varepsilon\frac{(z-1)z}{(1+z)^3}$		
$f^1(2,0)$	$\frac{1}{\varepsilon}(-y+\frac{z}{1+z})$			$-\varepsilon^2\frac{z(1-4z+z^2)}{(1+z)^4}$	
$\vdots$	$\vdots$	$\vdots$	$\vdots$	$\vdots$	$\vdots$
$f^1(\infty,0)$	$\frac{1}{\varepsilon}(-y+\frac{z}{1+z})$				
f^1_{Eige}	$\frac{1}{\varepsilon}(-y+\frac{z}{1+z})$		$+\varepsilon\frac{2z^2}{(1+z)^3}$	$+\varepsilon^2\frac{2z^2}{(1+z)^3}$	$+\varepsilon^3\frac{2z^2}{(1+z)^3}\ldots$

The table shows how the first mode amplitude f^1 changes with B^r-refinements.

Table 7
Coefficients of the z^n expansion of the manifolds for case (ii) (time derivatives included) and $B^r(0,0) = I$

(k,m)	z	z^2	z^3	z^4
$(0,0)$	$1-\varepsilon$	$-1+2\varepsilon$	$1-3\varepsilon$	$-1+4\varepsilon\ldots$
$(1,0)$	$1-\varepsilon^2$	$-1+4\varepsilon^2$	$1-9\varepsilon^2$	$-1+16\varepsilon^2\ldots$
$(2,0)$	$1-\varepsilon^3$	$-1+8\varepsilon^3$	$1-27\varepsilon^3$	$-1+64\varepsilon^3\ldots$
$\vdots$	$\vdots$	$\vdots$	$\vdots$	$\vdots$
$(\infty,0)$	1	-1	1	-1
Exact	1	-1	1	-1
Eige	1	$-1+2(\varepsilon^2+O(\varepsilon^3))$	$1-6(\varepsilon^2+O(\varepsilon^3))$	$-1+12(\varepsilon^2+O(\varepsilon^3))$

Each CSP refinement captures one higher order term in the manifold expansion, while using the eigenvectors as basis vectors capture correctly only the linear term.

$$k^f = [k_1^f, k_2^f, k_3^f] = \left[\frac{5}{\varepsilon}, \frac{1}{\varepsilon}, 1\right], \tag{82}$$

$$k^b = [k_1^b, k_2^b, k_3^b] = \left[\frac{5}{\varepsilon}, \frac{1}{\varepsilon}, 1\right], \tag{83}$$

where ε is a small parameter. The set of ODEs describing the evolution of Eq. (81) is thus

$$\frac{d\mathbf{W}}{dt} = \boldsymbol{g}, \tag{84}$$

where the vector of the unknown is defined as $\mathbf{W} = (X, Y, Z)^T$ and the right-hand side of (84) as

$$\boldsymbol{g} = \begin{bmatrix} -\frac{5X}{\varepsilon} - \frac{XY}{\varepsilon} + YZ + \frac{5Y^2}{\varepsilon} + \frac{Z}{\varepsilon} - X \\ 10\frac{X}{\varepsilon} - \frac{XY}{\varepsilon} - YZ - 10\frac{Y^2}{\varepsilon} + \frac{Z}{\varepsilon} + X \\ \frac{XY}{\varepsilon} - YZ - \frac{Z}{\varepsilon} + X \end{bmatrix}. \tag{85}$$

Solutions of Eq. (84) are obtained by numerical integration using the LSODE package [2]. The three eigenvalues of the Jacobian of $\boldsymbol{g}$ are computed and found real and negative. The time evolution of the three time scales (reciprocals of the absolute of the eigenvalues) are shown in Fig. 3: the first two fastest time scales are much faster than the third one.

As clearly shown in Fig. 4, in the phase space (X, Y, Z), any solution trajectory is attracted towards a 1-D manifold (a line in a 3-D phase space), after having experienced a fast initial transient during which the two (fast) mode amplitudes associated with the two fast time scales vanish (the time scales becoming "exhausted").

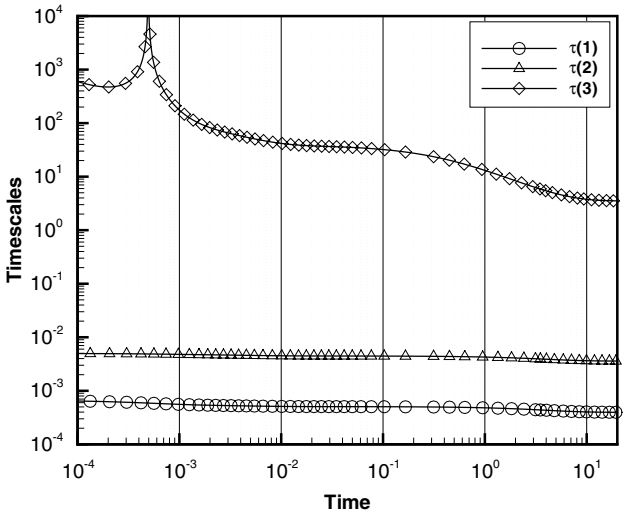

Fig. 3. Time scales (reciprocals of the absolute of the eigenvalues of J) corresponding to the eigenvectors of J; $\varepsilon = 0.01$, $X(0) = 0.5$, $Y(0) = 0.5$, $Z(0) = 0.5$.

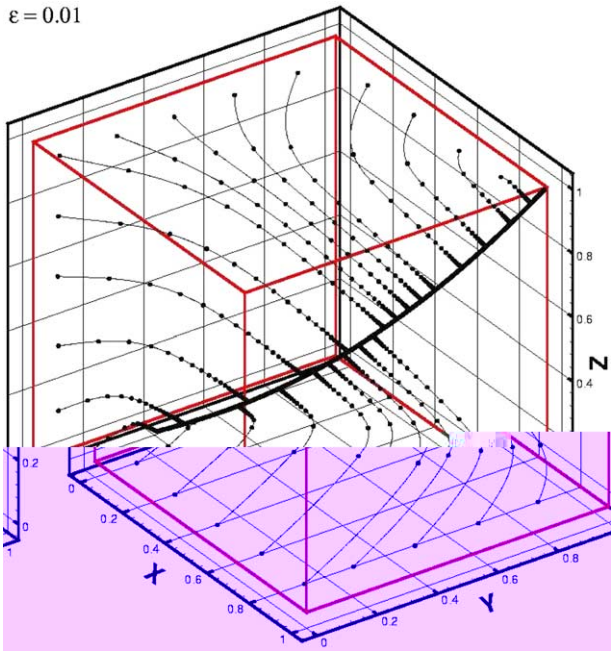

Fig. 4. All solution trajectories in the phase space are attracted by a 1-D manifold; markers are drawn at constant time intervals; $\varepsilon = 0.01$.

The problem at hand, being 3-dimensional, can be cast in CSP form as

$$\frac{\mathrm{d}\mathbf{W}}{\mathrm{d}t} = \boldsymbol{a}_1 f^1 + \boldsymbol{a}_2 f^3 + \boldsymbol{a}_3 f^3, \tag{86}$$

where $\boldsymbol{a}_1$, $\boldsymbol{a}_2$ and $\boldsymbol{a}_3$ are 3-dimensional column CSP vectors, and the f^i are the corresponding mode amplitudes. As the fastest time scale becomes exhausted, the amplitude f^1 becomes negligible, i.e. $f^1 \approx 0$ ($M = 1$). Similarly, when the second fastest time scale becomes exhausted, both amplitudes f^1 and f^2 become negligible, i.e. $f^1 \approx 0$ and $f^2 \approx 0$ ($M = 2$). In order for the simplified problem to provide a pre-specified accuracy, the first two modes are declared exhausted if the following conditions are met:

$$\begin{aligned} &\tau_2|\boldsymbol{a}_1 f^1| < \varepsilon_{\mathrm{rel}}|\mathbf{W}| + \varepsilon_{\mathrm{abs}}, \\ &\tau_3|\boldsymbol{a}_1 f^1 + \boldsymbol{a}_2 f^2| < \varepsilon_{\mathrm{rel}}|\mathbf{W}| + \varepsilon_{\mathrm{abs}}, \end{aligned} \tag{87}$$

where $|\mathbf{v}|$ denotes the absolute value of the elements of the vector $\mathbf{v}$, τ_2 and τ_3 are the second and third time scales, respectively, $\varepsilon_{\mathrm{rel}}$ is the relative error and $\varepsilon_{\mathrm{abs}}$ is the absolute error. In the numerical results that will be reported next, $\varepsilon_{\mathrm{rel}} = 1\mathrm{e}{-03}$ and $\varepsilon_{\mathrm{abs}} = 1\mathrm{e}{-10}$.

A leading order approximation of the 1-D manifold can be obtained algebraically by employing the left eigenvectors of J as the vectors $\boldsymbol{b}^i$ and by setting the two fastest modal amplitudes f^1, f^2 equal to zero:

$$f^1 = \boldsymbol{b}^1 \cdot \boldsymbol{g} = 0, \quad f^2 = \boldsymbol{b}^2 \cdot \boldsymbol{g} = 0 \tag{88}$$

yielding

$$\begin{aligned} Z &= \frac{X}{Y} - \frac{5\left(-X + Y^2\right)\left(1 + 3X + 4Y + 6Y^2\right)}{2Y\left(X + 2Y + 2Y^2\right)\varepsilon}, \\ Z &= \frac{X}{Y} + \frac{-X - 3X^2 - 4XY - 5XY^2 + 3X^2Y^2 + 4XY^3 + 6XY^4}{Y\left(1 + 3X + 4Y + 6Y^2 + Y\varepsilon + XY\varepsilon + 4Y^2\varepsilon + 2Y^3\varepsilon\right)}. \end{aligned} \tag{89}$$

The solution of the set of two algebraic equations, Eq. (88), is the intersection of the two surfaces in the 3-D phase plane as shown in Fig. 5. It is also apparent how the trajectory in Fig. 5 progressively relaxes at the intersection of the two surfaces as soon as the two fastest modes, associated with the two fastest time scales, become exhausted one after the other.

As with the Davis–Skodje problem, we will apply the CSP vector refinement procedure to this 3-species dynamical system. In this model problem, the CSP vectors can be found both algebraically or numerically by adopting the algorithms presented in Sections 4 and 5. A number of different refinement strategies can be envisaged, each diversified on the basis of (i) the choice of the initial basis vectors, (ii) the number of initial refinements not including the basis vectors time derivatives, and (iii) whether a final refinement including time derivatives is carried out. Table 8 summarizes all the different strategies considered here.

As for the Davis–Skodje problem, the effectiveness of CSP vector refinements will be gauged by inspection of the evolution of the ensuing CSP fast modal amplitudes along a given trajectory. We chose a trajectory corresponding to initial condition $X_0 = Y_0 = Z_0 = 0.5$ and $\varepsilon = 0.01$.

Method 1 involves using the eigenvectors of J as CSP vectors. Although not yielding the best choice of vectors but just their leading order approximation, we adopted the results of this method (reported in Figs. 6 and 7) as a reference enabling us to compare all other methods described in Table 8.

First, we want to assess that the CSP refinements, when the contribution of the time derivatives of the CSP vectors is not included, converge to the results of Method 1 (Phase (1) only, Section 4). To this aim, Method 3 and 4 involve a number (1, 2, or 4) of CSP refinements wherein the contribution of the time derivatives of the CSP vectors is not included, adopting as initial basis the identity matrix and a randomly chosen matrix, respectively.

Fig. 6 shows that the amplitude of the first of the fast modes f^1 initially exhibits a fast decrease under the action of the two fast time scales until it reaches the asymptotic value $\boldsymbol{f}^1_\infty$, estimated according to the expression Eq. (A.30):

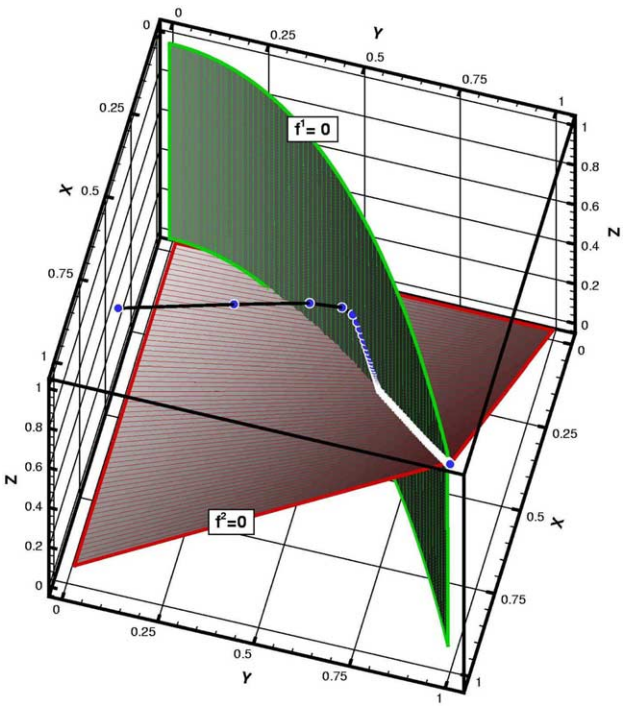

Fig. 5. 1-D manifold defined as the intersection of the two surfaces defined by Eqs. (88) or (89).

Table 8
List of refinement strategies (methods) and of the associated algorithmic options

Method	Initial basis	No. of refinements: $\frac{dJ}{dt} = 0$	No. of refinements: $\frac{dJ}{dt} \neq 0$
1	Eigenvectors	0	0
2	Eigenvectors	0	1 (M fixed)
3	Identity	1, 2, 4	0
4	Random	1, 2, 4	0

$$\boldsymbol{f}^{r}_{\infty} \approx -\sum_{r'=1,M} T^{r}_{r'} \Lambda^{r'}_{s} \boldsymbol{f}^{s}, \quad s = M+1, 3.$$

From this expression is apparent that $\boldsymbol{f}^{r}_{\infty}$ can theoretically vanish providing a perfect decoupling of the fast and slow subspace be obtainable via ideal basis vectors (e.g. $\Lambda^{r'}_{s} = 0$). Otherwise $\boldsymbol{f}^{r}_{\infty}$ evolves according to the (slow) time scales of the slow amplitudes $\boldsymbol{f}^{s}$. Indeed, that the latter circumstance is the one occurring when the approximations of the ideal vectors as offered by the CSP refinements are adopted can be appreciated by noting in Fig. 6, and also in Fig. 7, that the magnitude of f^1, past a large drop on a short time period (fast time scale), stays leveled at a small value for a long time period (slow time scale) hindered in its further reduction by the action of the residual coupling with the slow time scales, and only at large times it eventually vanishes as the system reaches equilibrium. A qualitatively similar behavior is observed for the amplitude of the second of the fast modes f^2, although no data have been demonstrated here. The amplitude of the third (slow) mode f^3 evolves at all times with the slowest time scale.

It is clear from Fig. 6 that the evolution of the fast amplitude f^1 as obtained by Method 3 and 4 converge to that obtained by Method 1. This result may be thought of as the numerical counterpart of the analytic results obtained for the Davis–Skodje problem and displayed in Table 4.

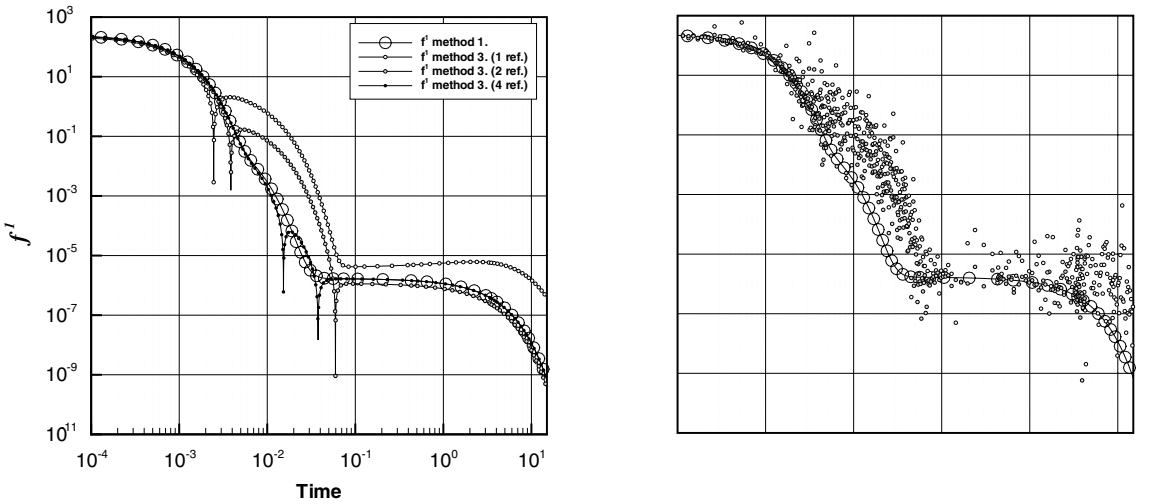

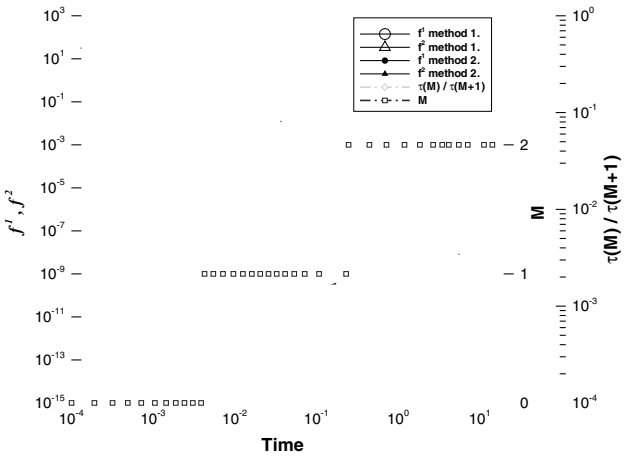

Fig. 7. Method 2. Single refinement of the eigenvector basis with fixed $\tilde{M}$.

Next, we want to assess the effect of the CSP refinements when the contribution of the time derivatives of the CSP vectors is included. To this aim, Method 2 involves starting with the eigenvector basis (as in Method 1), then finding the number of exhausted modes $\tilde{M}$ with respect to this basis, and finally carrying out one CSP refinement wherein the contribution of the time derivatives of the CSP vectors is included (Phase (2), see Section 4) *and* assuming $M = \tilde{M}$. Fig. 7 shows the number $\tilde{M}$ of exhausted modes found by Method 1, according to the criteria (87), and the evolution of the fast amplitudes f^1 and f^2 as obtained by Methods 1 and 2. Since the refinement procedure affects only the first M modes, by the consideration of the time derivatives of the CSP vectors, then when $\tilde{M} = 1, f^1$ is affected and f^2 is not, while when $\tilde{M} = 2$, both f^1 and f^2 are affected. It is shown that consideration of the time derivative terms does indeed allow the amplitudes f^1 and f^2 to drop to much lower values; so that a more accurate description of the manifold is obtained.

7. Conclusions

Given that (i) it has been proved [23] that the CSP method can provide high-order approximations of the slow invariant manifolds (SIM) characterizing the dynamics of stiff system of ODEs, and (ii) the CSP refinements provide high-order accuracy for a nonlinear problem only when the time rates of change of the CSP vectors are properly accounted for [18–20], and finally (iii) thus far, no specific analysis was available in the literature on how to evaluate the time rates of change of the CSP vectors, the aim of this paper has been to derive the formulae needed to evaluate the time rates of change of the CSP vectors whenever these terms cannot be computed algebraically.

With reference to two simple model problems, we showed that, by adopting these formulae, the iterative procedures of CSP refinements, illustrated in Sections 3 and 4, yield the asymptotic expansion of the SIM in powers of the spectral gap, the small parameter in the singular perturbation analysis of these fast/slow systems.

We also showed that Phase (2) of the B^r-refinement requires the availability of the time rate of change of the Jacobian matrix $\mathrm{d}J/\mathrm{d}t$ of the RHS of the set of ODEs describing the system dynamics, while the A_r-refinement requires the availability of both $\mathrm{d}J/\mathrm{d}t$ and $\mathrm{d}^2J/\mathrm{d}t^2$. We have also shown that $\mathrm{d}J/\mathrm{d}t$ and $\mathrm{d}^2J/\mathrm{d}t^2$ depend on the state of the system only, and that they are local measures of the geometrical characteristics of the manifold (such as local curvature and higher order terms), since they involve the terms $\partial J/\partial y^i$ and $\partial^2 J/\partial y^i \partial y^j$. As a consequence, the time rates of change of the CSP vectors also depend exclusively on the local state variables. Hence, tabulation methods, such as PRISM [32] or ISAT [33], can be used to generate look-up tables for SIMs of high-order accuracy found by means of the CSP refinement procedure.

We presented both analytical and numerical evidence of the CSP performance. Regarding the numerics, we showed that, in practice, only one or (rarely) two CSP refinements can be performed, if the time rates of change of the CSP vectors are taken into account. Here, the limitations, solely related to issues of computational efficiency and not of theoretical nature, are set by the need to have available high-order time derivatives of the Jacobian.

Acknowledgments

This work was supported by the US Department of Energy (DOE), Office of Basic Energy Sciences (BES), SciDAC Computational Chemistry Program. Support was also provided by the DOE BES Division of Chemical Sciences, Geosciences, and Biosciences. Sandia National Laboratories is a multiprogram laboratory operated by Sandia Corporation, a Lockheed Martin Company, for the United States Department of Energy under contract DE-AC04-94-AL85000. M.Valorani also acknowledges the support of the Italian Space Agency (ASI) and the Italian Ministry of Education, University and Research (MIUR).

Appendix A

A.1. The B^r-refinement

The evolution of the mode amplitudes f^i is governed by the equations:

$$\frac{\mathrm{d}f^i}{\mathrm{d}t} = \sum_{j=1,N} \Lambda^i_j f^j, \quad i = 1, N. \tag{A.1}$$

Given a set of basis vectors at the (k, m)-th refinement level and Eq. (A.1), one can recast the evolution of the fast amplitudes as

$$\frac{\mathrm{d}\boldsymbol{f}^r(k,m)}{\mathrm{d}t} = \Lambda_r^r(k,m)\boldsymbol{f}^r(k,m) + \Lambda_s^r(k,m)\boldsymbol{f}^s(k,m), \tag{A.2}$$

where

$$\Lambda_r^r(k,m) = \left(\frac{\mathrm{d}B^r(k,m)}{\mathrm{d}t} + B^r(k,m)J\right)A_r(k,m), \tag{A.3}$$

$$\Lambda_s^r(k,m) = \left(\frac{\mathrm{d}B^r(k,m)}{\mathrm{d}t} + B^r(k,m)J\right)A_s(k,m), \tag{A.4}$$

and $T_r^r(k,m)$ is the inverse of $\Lambda_r^r(k,m)$. Recasting Eq. (A.2) as

$$\frac{\mathrm{d}\boldsymbol{f}^r(k,m)}{\mathrm{d}t} = \Lambda_r^r(k,m)\left(\boldsymbol{f}^r(k,m) + T_r^r(k,m)\Lambda_s^r(k,m)\boldsymbol{f}^s(k,m)\right), \tag{A.5}$$

it is seen that the asymptotic limit for $\boldsymbol{f}^r(k,m)$ is

$$\boldsymbol{f}^r(k,m) \approx -T_r^r(k,m)\Lambda_s^r(k,m)\boldsymbol{f}^s(k,m). \tag{A.6}$$

Wishing to make the amplitudes in $\boldsymbol{f}^r$ as small as possible in the period where the fast time scales are exhausted, Eq. (A.5) suggests that a new set of fast amplitudes be defined as

$$\boldsymbol{f}^r(k+1,m) = \boldsymbol{f}^r(k,m) + T_r^r(k,m)\Lambda_s^r(k,m)\boldsymbol{f}^s(k,m). \tag{A.7}$$

This is equivalent of defining a new set of basis vectors as

$$B^r(k+1,m) = T_r^r(k,m)\left(\frac{\mathrm{d}B^r(k,m)}{\mathrm{d}t} + B^r(k,m)J\right), \tag{A.8}$$

$$A_r(k+1,m) = A_r(k,m), \tag{A.9}$$

$$B^s(k+1,m) = B^s(k,m), \tag{A.10}$$

$$A_s(k+1,m) = \left[I_r^r - A_r(k+1,m)B^r(k+1,m)\right]A_s(k,m), \tag{A.11}$$

where the last relation is required to restore the orthogonality between $A_s(k+1,m)$ and the new, rotated $B^r(k+1,m)$ basis vector.

A.2. The A_r-refinement

According to Eq. (A.1), at the (k,m) refinement level the evolution of the slow amplitudes is governed by the equations:

$$\frac{\mathrm{d}\boldsymbol{f}^s(k,m)}{\mathrm{d}t} = \Lambda_r^s(k,m)\boldsymbol{f}^r(k,m) + \Lambda_s^s(k,m)\boldsymbol{f}^s(k,m), \tag{A.12}$$

where

$$\Lambda_r^s(k,m) = \left(\frac{\mathrm{d}B^s(k,m)}{\mathrm{d}t} + B^s(k,m)J\right)A_r(k,m), \tag{A.13}$$

$$\Lambda_s^s(k,m) = \left(\frac{\mathrm{d}B^s(k,m)}{\mathrm{d}t} + B^s(k,m)J\right)A_s(k,m). \tag{A.14}$$

Wishing to limit the influence of the fast time scales to the evolution of the slow amplitudes, Eq. (A.12) is recast as

$$\begin{aligned}&\frac{\mathrm{d}\left[\boldsymbol{f}^s(k,m) - \Lambda_r^s(k,m)T_r^r(k,m)\boldsymbol{f}^r(k,m)\right]}{\mathrm{d}t}\\ &\quad= -\frac{\mathrm{d}\Lambda_r^s(k,m)T_r^r(k,m)}{\mathrm{d}t}\boldsymbol{f}^r(k,m) + \left[\Lambda_s^s(k,m) - \Lambda_r^s(k,m)T_r^r(k,m)\Lambda_s^r(k,m)\right]\boldsymbol{f}^s(k,m)\end{aligned} \tag{A.15}$$

suggesting that a new set of slow amplitudes be defined as

$$\boldsymbol{f}^s(k,m+1) = \boldsymbol{f}^s(k,m) - \Lambda_r^s(k,m)T_r^r(k,m)\boldsymbol{f}^r(k,m). \tag{A.16}$$

This is equivalent of defining a new set of basis vectors as

$$A_r(k,m+1) = \left[-\frac{\mathrm{d}A_r(k,m)}{\mathrm{d}t} + JA_r(k,m)\right] T_r^r(k,m), \tag{A.17}$$

$$B^r(k,m+1) = B^r(k,m), \tag{A.18}$$

$$B^s(k,m+1) = B^s(k,m)\left[I_r^r - A_r(k,m+1)B^r(k,m+1)\right], \tag{A.19}$$

$$A_s(k,m+1) = A_s(k,m). \tag{A.20}$$

A.3. Action of the refinements

The action of the B^r- and A_r-refinements, Eqs. (11)–(14) or (A.4)–(A.7) and (16)–(19) or (A.11)–(A.14), respectively, are clearly manifested if the magnitude of the matrices $\Lambda_r^r(k,m), \Lambda_s^r(k,m)$, $\Lambda_r^s(k,m)$ and $\Lambda_s^s(k,m)$ is examined, for increasing values of the refinement levels "k" and/or "m". As was shown previously, at the (k,m)-th refinement level the fast and slow amplitudes are governed by the equations:

$$\frac{\mathrm{d}\boldsymbol{f}^r(k,m)}{\mathrm{d}t} = \Lambda_r^r(k,m)\boldsymbol{f}^r(k,m) + \Lambda_s^r(k,m)\boldsymbol{f}^s(k,m), \tag{A.21}$$

$$\frac{\mathrm{d}\boldsymbol{f}^s(k,m)}{\mathrm{d}t} = \Lambda_r^s(k,m)\boldsymbol{f}^r(k,m) + \Lambda_s^s(k,m)\boldsymbol{f}^s(k,m). \tag{A.22}$$

At this point it is assumed that

$$\|T_r^r(k,m)\| \approx \mathrm{O}(\tau_M), \quad \|\Lambda_s^s(k,m)\| \approx \mathrm{O}(1/\tau_{M+1}), \tag{A.23}$$

where τ_i is the i-th time scale in the problem.

A single B^r-refinement yields

$$\Lambda_r^r(k+1,m) = \Lambda_r^r(k,m) + T_r^r(k,m)\Lambda_s^r(k,m)\Lambda_r^s(k,m), \tag{A.24}$$

$$\Lambda_s^r(k+1,m) = \frac{\mathrm{d}\left[T_r^r(k,m)\Lambda_s^r(k,m)\right]}{\mathrm{d}t} + \left[T_r^r(k,m)\Lambda_s^r(k,m)\right]\Lambda_s^s(k+1,m), \tag{A.25}$$

$$\Lambda_r^s(k+1,m) = \Lambda_r^s(k,m), \tag{A.26}$$

$$\Lambda_s^s(k+1,m) = \Lambda_s^s(k,m) - \Lambda_r^s(k,m)T_r^r(k,m)\Lambda_s^r(k,m). \tag{A.27}$$

According to the estimates (A.23) and the fact that the fastest non-exhausted time scale is τ_{M+1}, Eq. (A.25) suggests that

$$\|\Lambda_s^r(k+1,m)\| \approx \mathrm{O}\left(\frac{\tau_M}{\tau_{cur}}\Lambda_s^r(k,m)\right) + \mathrm{O}\left(\frac{\tau_M}{\tau_{M+1}}\Lambda_s^r(k,m)\right), \tag{A.28}$$

where the two terms on the RHS correspond to the two terms in the RHS of Eq. (A.25) and τ_{cur} is the currently dominant time scale. Since the M fastest time scales are exhausted, it follows that $\tau_{cur} \geqslant \tau_{M+1}$ so that Eq. (30a) simplifies to

$$\|\Lambda_s^r(k+1,m)\| \approx \mathrm{O}\left(\varepsilon\Lambda_s^r(k,m)\right), \tag{A.29}$$

where $\varepsilon = \tau_M/\tau_{M+1}$ is a measure of the fast/slow time scale separation. Eq. (A.29) indicates that the coupling of the fast amplitudes to the slow ones in Eq. (A.21) decreases by an order of ε each time a B^r-refinement is

performed. In contrast, the coupling of the slow amplitudes to the fast ones in Eq. (A.22) stays unaffected. Since, as Eq. (A.21) shows, the asymptotic value of $\boldsymbol{f}^r(k,m)$ is

$$\boldsymbol{f}^r(k,m) \approx -T_r^r(k,m)\Lambda_s^r(k,m)\boldsymbol{f}^s(k,m), \tag{A.30}$$

the additional B^r-refinement allows the fast amplitudes to decrease to a lower value. In view of the simplified problem (10), such a refinement allows the computation of a more accurate solution.

Similarly, one A_r-refinement yields

$$\Lambda_r^r(k,m+1) = \Lambda_r^r(k,m) + \Lambda_s^r(k,m)\Lambda_r^s(k,m)T_r^r(k,m), \tag{A.31}$$
$$\Lambda_s^r(k,m+1) = \Lambda_s^r(k,m), \tag{A.32}$$
$$\Lambda_r^s(k,m+1) = -\frac{\mathrm{d}\left[\Lambda_r^s(k,m)T_r^r(k,m)\right]}{\mathrm{d}t} + \Lambda_s^s(k,m+1)\left[\Lambda_r^s(k,m)T_r^r(k,m)\right], \tag{A.33}$$
$$\Lambda_s^s(k,m+1) = \Lambda_s^s(k,m) - \Lambda_r^s(k,m)T_r^r(k,m)\Lambda_s^r(k,m). \tag{A.34}$$

These relations suggest that

$$\|\Lambda_r^s(k,m+1)\| \approx \mathrm{O}\left(\varepsilon\Lambda_r^s(k,m)\right), \tag{A.35}$$

i.e. the coupling of the slow amplitudes to the fast ones in Eq. (A.22) decreases by an order of ε each time an A_r-refinement is performed, making the simplified problem (10) less stiff. However, since the coupling of the fast amplitudes to the slow ones in Eq. (A.21) is not affected, the accuracy of the simplified problem is not improved.

Appendix B. CSP vector time derivative derivation

The CSP vector time derivatives are obtained by means of chain rule differentiation of the relations illustrated in Section 4. In the following we summarize the main results.

Given that

$$\frac{\mathrm{d}\lambda_r^r(0,0)}{\mathrm{d}t} = \frac{\mathrm{d}}{\mathrm{d}t}\left[\left(\frac{\mathrm{d}B^r(0,0)}{\mathrm{d}t} + B^r(0,0)J\right)A_r(0,0)\right] = \frac{\mathrm{d}}{\mathrm{d}t}\left[B^r(0,0)JA_r(0,0)\right] = B^r(0,0)\frac{\mathrm{d}J}{\mathrm{d}t}A_r(0,0), \tag{B.1}$$
$$\frac{\mathrm{d}\tau_r^r(0,0)}{\mathrm{d}t} = -\tau_r^r(0,0)\frac{\mathrm{d}\lambda_r^r(0,0)}{\mathrm{d}t}\tau_r^r(0,0) = -\tau_r^r(0,0)B^r(0,0)\frac{\mathrm{d}J}{\mathrm{d}t}A_r(0,0)\tau_r^r(0,0), \tag{B.2}$$

then the time derivative of $B^r(1,0)$ and $B^r(1,1)$ can be evaluated as

$$\begin{aligned}
\frac{\mathrm{d}B^r(1,1)}{\mathrm{d}t} &= \frac{\mathrm{d}B^r(1,0)}{\mathrm{d}t} \\
&= \frac{\mathrm{d}\tau_r^r(0,0)}{\mathrm{d}t}B^r(0,0)J + \tau_r^r(0,0)B^r(0,0)\frac{\mathrm{d}J}{\mathrm{d}t} \\
&= -\tau_r^r(0,0)B^r(0,0)\frac{\mathrm{d}J}{\mathrm{d}t}A_r(0,0)\tau_r^r(0,0)B^r(0,0)J + \tau_r^r(0,0)B^r(0,0)\frac{\mathrm{d}J}{\mathrm{d}t} \\
&= -\tau_r^r(0,0)B^r(0,0)\frac{\mathrm{d}J}{\mathrm{d}t}A_r(0,0)B^r(1,0) + \tau_r^r(0,0)B^r(0,0)\frac{\mathrm{d}J}{\mathrm{d}t} \\
&= \tau_r^r(0,0)B^r(0,0)\frac{\mathrm{d}J}{\mathrm{d}t}\left[I - A_r(0,0)B^r(1,0)\right].
\end{aligned} \tag{B.3}$$

Moreover, given that

$$\begin{aligned}
\frac{\mathrm{d}\lambda_r^r(1,0)}{\mathrm{d}t} &= \frac{\mathrm{d}}{\mathrm{d}t}\left[B^r(1,0)JA_r(0,0)\right] = \frac{\mathrm{d}B^r(1,0)}{\mathrm{d}t}JA_r(0,0) + B^r(1,0)\frac{\mathrm{d}J}{\mathrm{d}t}A_r(0,0),\\
\frac{\mathrm{d}\tau_r^r(1,0)}{\mathrm{d}t} &= -\tau_r^r(1,0)\frac{\mathrm{d}\lambda_r^r(1,0)}{\mathrm{d}t}\tau_r^r(1,0)\\
&= -\tau_r^r(1,0)\frac{\mathrm{d}B^r(1,0)}{\mathrm{d}t}JA_r(0,0)\tau_r^r(1,0) - \tau_r^r(1,0)B^r(1,0)\frac{\mathrm{d}J}{\mathrm{d}t}A_r(0,0)\tau_r^r(1,0)\\
&= -\tau_r^r(1,0)\frac{\mathrm{d}B^r(1,0)}{\mathrm{d}t}A_r(1,1) - \tau_r^r(1,0)B^r(1,0)\frac{\mathrm{d}J}{\mathrm{d}t}A_r(0,0)\tau_r^r(1,0),
\end{aligned} \tag{B.4}$$

then the time derivative of $A_r(1,1)$ and $A_r(2,1)$ can be evaluated as

$$\begin{aligned}
\frac{\mathrm{d}A_r(1,1)}{\mathrm{d}t} &= \frac{\mathrm{d}A_r(2,1)}{\mathrm{d}t}\\
&= \frac{\mathrm{d}}{\mathrm{d}t}\left[JA_r(0,0)\tau_r^r(1,0)\right] = \frac{\mathrm{d}J}{\mathrm{d}t}A_r(0,0)\tau_r^r(1,0) + J\frac{\mathrm{d}A_r(0,0)}{\mathrm{d}t}\tau_r^r(1,0) + JA_r(0,0)\frac{\mathrm{d}\tau_r^r(1,0)}{\mathrm{d}t}\\
&= \frac{\mathrm{d}J}{\mathrm{d}t}A_r(0,0)\tau_r^r(1,0) - JA_r(0,0)\tau_r^r(1,0)\frac{\mathrm{d}B^r(1,0)}{\mathrm{d}t}A_r(1,1)\\
&\quad - JA_r(0,0)\tau_r^r(1,0)B^r(1,0)\frac{\mathrm{d}J}{\mathrm{d}t}A_r(0,0)\tau_r^r(1,0)\\
&= \frac{\mathrm{d}J}{\mathrm{d}t}A_r(0,0)\tau_r^r(1,0) - A_r(1,1)\frac{\mathrm{d}B^r(1,0)}{\mathrm{d}t}A_r(1,1) - A_r(1,0)B^r(1,0)\frac{\mathrm{d}J}{\mathrm{d}t}A_r(0,0)\tau_r^r(1,0),\\
&= \left[I - A_r(1,1)B^r(1,0)\right]\frac{\mathrm{d}J}{\mathrm{d}t}A_r(0,0)\tau_r^r(1,0) - A_r(1,1)\frac{\mathrm{d}B^r(1,0)}{\mathrm{d}t}A_r(1,1).
\end{aligned} \tag{B.5}$$

It follows that the time derivative of $B^r(2,1)$ can be evaluated as

$$\begin{aligned}
\frac{\mathrm{d}B^r(2,1)}{\mathrm{d}t} &= \frac{\mathrm{d}}{\mathrm{d}t}\left[\tau_r^r(1,1)\left(\frac{\mathrm{d}B^r(1,0)}{\mathrm{d}t} + B^r(1,0)J\right)\right]\\
&= \frac{\mathrm{d}\tau_r^r(1,1)}{\mathrm{d}t}\frac{\mathrm{d}B^r(1,0)}{\mathrm{d}t} + \tau_r^r(1,1)\frac{\mathrm{d}^2B^r(1,0)}{\mathrm{d}t^2} + \frac{\mathrm{d}\tau_r^r(1,1)}{\mathrm{d}t}B^r(1,1)J + \tau_r^r(1,1)\frac{\mathrm{d}B^r(1,0)}{\mathrm{d}t}J\\
&\quad + \tau_r^r(1,1)B^r(1,0)\frac{\mathrm{d}J}{\mathrm{d}t}\\
&= \frac{\mathrm{d}\tau_r^r(1,1)}{\mathrm{d}t}\left[\frac{\mathrm{d}B^r(1,0)}{\mathrm{d}t} + B^r(1,1)J\right] + \tau_r^r(1,1)\frac{\mathrm{d}^2B^r(1,0)}{\mathrm{d}t^2} + \tau_r^r(1,1)\frac{\mathrm{d}B^r(1,0)}{\mathrm{d}t}J\\
&\quad + \tau_r^r(1,1)B^r(1,1)\frac{\mathrm{d}J}{\mathrm{d}t}\\
&= \frac{\mathrm{d}\tau_r^r(1,1)}{\mathrm{d}t}\lambda_r^r(1,1)B^r(2,1) + \tau_r^r(1,1)\frac{\mathrm{d}^2B^r(1,0)}{\mathrm{d}t^2} + \tau_r^r(1,1)\frac{\mathrm{d}B^r(1,0)}{\mathrm{d}t}J\\
&\quad + \tau_r^r(1,1)B^r(1,1)\frac{\mathrm{d}J}{\mathrm{d}t},
\end{aligned} \tag{B.6}$$

where

$$\begin{aligned}\frac{\mathrm{d}\tau_r^r(1,1)}{\mathrm{d}t} &= -\tau_r^r(1,1)\frac{\mathrm{d}\lambda_r^r(1,1)}{\mathrm{d}t}\tau_r^r(1,1)\\ &= -\tau_r^r(1,1)\frac{\mathrm{d}}{\mathrm{d}t}\left[\left(\frac{\mathrm{d}B^r(1,0)}{\mathrm{d}t}+B^r(1,0)J\right)A_r(1,1)\right]\tau_r^r(1,1)\\ &= -\tau_r^r(1,1)\left[\frac{\mathrm{d}^2B^r(1,0)}{\mathrm{d}t^2}A_r(1,1)+\frac{\mathrm{d}B^r(1,0)}{\mathrm{d}t}\frac{\mathrm{d}A_r(1,1)}{\mathrm{d}t}+B^r(1,0)\frac{\mathrm{d}J}{\mathrm{d}t}A_r(1,1)\right.\\ &\quad\left.+B^r(1,0)J\frac{\mathrm{d}A_r(1,1)}{\mathrm{d}t}+\frac{\mathrm{d}B^r(1,0)}{\mathrm{d}t}JA_r(1,1)\right]\tau_r^r(1,1).\end{aligned} \tag{B.7}$$

Replacing Eq. (B.6) in Eq. (B.7) yields

$$\begin{aligned}\frac{\mathrm{d}B^r(2,1)}{\mathrm{d}t} &= -\tau_r^r(1,1)\frac{\mathrm{d}^2B^r(1,0)}{\mathrm{d}t^2}A_r(1,1)B^r(2,1)-\tau_r^r(1,1)\frac{\mathrm{d}B^r(1,0)}{\mathrm{d}t}\frac{\mathrm{d}A_r(1,1)}{\mathrm{d}t}B^r(2,1)\\ &\quad-\tau_r^r(1,1)B^r(1,0)\frac{\mathrm{d}J}{\mathrm{d}t}A_r(1,1)B^r(2,1)-\tau_r^r(1,1)B^r(1,0)J\frac{\mathrm{d}A_r(1,1)}{\mathrm{d}t}B^r(2,1)-\tau_r^r(1,1)\\ &\quad\times\frac{\mathrm{d}B^r(1,0)}{\mathrm{d}t}JA_r(1,1)B^r(2,1)+\tau_r^r(1,1)\frac{\mathrm{d}^2B^r(1,0)}{\mathrm{d}t^2}+\tau_r^r(1,1)\frac{\mathrm{d}B^r(1,0)}{\mathrm{d}t}J\\ &\quad+\tau_r^r(1,1)B^r(1,1)\frac{\mathrm{d}J}{\mathrm{d}t}.\end{aligned} \tag{B.8}$$

After regrouping, one obtains

$$\begin{aligned}\frac{\mathrm{d}B^r(2,1)}{\mathrm{d}t} &= \tau_r^r(1,1)\left[\frac{\mathrm{d}B^r(1,0)}{\mathrm{d}t}J+B^r(1,0)\frac{\mathrm{d}J}{\mathrm{d}t}+\frac{\mathrm{d}^2B^r(1,0)}{\mathrm{d}t^2}\right][I-A_r(1,1)B^r(2,1)]\\ &\quad-\tau_r^r(1,1)\left[\frac{\mathrm{d}B^r(1,0)}{\mathrm{d}t}+B^r(1,0)J\right]\frac{\mathrm{d}A_r(1,1)}{\mathrm{d}t}B^r(2,1).\end{aligned} \tag{B.9}$$

From

$$\frac{\mathrm{d}B^r(1,0)}{\mathrm{d}t}+B^r(1,0)J=\lambda_r^r(1,1)B^r(2,1), \tag{B.10}$$

one obtains

$$\begin{aligned}\frac{\mathrm{d}B^r(2,1)}{\mathrm{d}t} &= \tau_r^r(1,1)\left[\frac{\mathrm{d}B^r(1,0)}{\mathrm{d}t}J+B^r(1,0)\frac{\mathrm{d}J}{\mathrm{d}t}+\frac{\mathrm{d}^2B^r(1,0)}{\mathrm{d}t^2}\right][I-A_r(1,1)B^r(2,1)]\\ &\quad-B^r(2,1)\frac{\mathrm{d}A_r(1,1)}{\mathrm{d}t}B^r(2,1).\end{aligned} \tag{B.11}$$

The second order time derivative of $B^r(1,0)$ can be obtained as

$$\begin{aligned}\frac{\mathrm{d}^2B^r(1,0)}{\mathrm{d}t^2} &= \frac{\mathrm{d}}{\mathrm{d}t}\left[\tau_r^r(0,0)B^r(0,0)\frac{\mathrm{d}J}{\mathrm{d}t}(I-A_r(0,0)B^r(1,0))\right]\\ &= \frac{\mathrm{d}\tau_r^r(0,0)}{\mathrm{d}t}B^r(0,0)\frac{\mathrm{d}J}{\mathrm{d}t}+\tau_r^r(0,0)B^r(0,0)\frac{\mathrm{d}^2J}{\mathrm{d}t^2}-\frac{\mathrm{d}\tau_r^r(0,0)}{\mathrm{d}t}B^r(0,0)\frac{\mathrm{d}J}{\mathrm{d}t}A_r(0,0)B^r(1,0)\\ &\quad-\tau_r^r(0,0)B^r(0,0)\frac{\mathrm{d}^2J}{\mathrm{d}t^2}A_r(0,0)B^r(1,0)-\tau_r^r(0,0)B^r(0,0)\frac{\mathrm{d}J}{\mathrm{d}t}A_r(0,0)\frac{\mathrm{d}B^r(1,0)}{\mathrm{d}t}.\end{aligned} \tag{B.12}$$

After regrouping, one obtains

$$\frac{\mathrm{d}^2 B^r(1,0)}{\mathrm{d}t^2} = \left[\frac{\mathrm{d}\tau_r^r(0,0)}{\mathrm{d}t} B^r(0,0)\frac{\mathrm{d}J}{\mathrm{d}t} + \tau_r^r(0,0)B^r(0,0)\frac{\mathrm{d}^2 J}{\mathrm{d}t^2}\right][I - A_r(0,0)B^r(1,0)] - \tau_r^r(0,0)B^r(0,0) \times \frac{\mathrm{d}J}{\mathrm{d}t} A_r(0,0)\frac{\mathrm{d}B^r(1,0)}{\mathrm{d}t}. \tag{B.13}$$

Additional formulae for terms not appearing in the refinement procedure but required for diagnostic purposes, e.g. in the evaluation of the off-diagonal blocks λ_s^r and λ_r^s are reported in the following:

$$\frac{\mathrm{d}A_s(1,0)}{\mathrm{d}t} = \frac{\mathrm{d}A_s(1,1)}{\mathrm{d}t} = \frac{\mathrm{d}}{\mathrm{d}t}[(I - A_r(0,0)B^r(1,0))A_s(0,0)] = -A_r(0,0)\frac{\mathrm{d}B^r(1,0)}{\mathrm{d}t}A_s(0,0),$$

$$\begin{aligned}\frac{\mathrm{d}B^s(1,1)}{\mathrm{d}t} = \frac{\mathrm{d}B^s(2,1)}{\mathrm{d}t} &= \frac{\mathrm{d}}{\mathrm{d}t}[B^s(1,0)(I - A_r(1,1)B^r(1,1))] \\ &= \frac{\mathrm{d}}{\mathrm{d}t}[B^s(0,0)(I - A_r(1,1)B^r(1,0))] \\ &= -B^s(0,0)\left[\frac{\mathrm{d}A_r(1,1)}{\mathrm{d}t}B^r(1,0) + A_r(1,1)\frac{\mathrm{d}B^r(1,0)}{\mathrm{d}t}\right],\end{aligned}$$

$$\begin{aligned}\frac{\mathrm{d}A_s(2,1)}{\mathrm{d}t} &= \frac{\mathrm{d}}{\mathrm{d}t}[(I - A_r(2,1)B^r(2,1))A_s(1,1)] = \frac{\mathrm{d}}{\mathrm{d}t}[(I - A_r(1,1)B^r(2,1))A_s(1,0)] \\ &= -\left[\frac{\mathrm{d}A_r(1,1)}{\mathrm{d}t}B^r(2,1) + A_r(1,1)\frac{\mathrm{d}B^r(2,1)}{\mathrm{d}t}\right]A_s(1,0) + (I - A_r(1,1)B^r(2,1))\frac{\mathrm{d}A_s(1,0)}{\mathrm{d}t}.\end{aligned}$$

References

[1] C. Gear, Numerical Initial Value Problems in Ordinary Differential Equations, Prentice-Hall, Englewood Cliffs, NJ, 1971.
[2] A.C. Hindmarsh, Odepack, a systematized collection of ODE solvers, in: R.S. Stepleman, et al. (Eds.), Scientific Computing, North-Holland, Amsterdam, 1983, p. 55.
[3] P. Brown, G. Byrne, A. Hindmarsh, VODE, a variable-coefficient ODE solver, Technical Report UCRL-98412, Lawrence Livermore National Laboratory, Livermore, CA; see also: SIAM J. Sci. Statist. Comput. 10 (1989) 1038–1051 (June 1988).
[4] P. Brown, A. Hindmarsh, Reduced storage matrix methods in stiff ODE systems, J. Appl. Math. Comput. 31 (1989) 40–91.
[5] D. Chapman, L. Underhill, J. Chem. Soc. Trans. 103 (1913) 496.
[6] M. Bodenstein, W. Dux, Photochemische kinetik des chlorknallgases, Z. Phys. Chem. 85 (1913) 329.
[7] A. Skrabal, Ann. Phys. 82 (1927) 138.
[8] J. Bowen, A. Acrivos, A. Oppenheim, Singular perturbation refinement to quasi-steady state approximation in chemical kinetics, Chem. Eng. Sci. 18 (1927) 177–188.
[9] F. Heineken, H. Tsuchiya, R. Aris, On the mathematical status of the pseudo-steady-state hypothesis of biochemical kinetics, Math. Biosci. 1 (1967) 95.
[10] S. Fraser, The steady state and equilibrium approximations: a geometrical picture, J. Chem. Phys. 88 (1988) 4732–4738.
[11] N. Fenichel, Geometric singular perturbation theory for ordinary differential equations, J. Differential Equation 31 (1977) 53.
[12] M. Roussel, S. Fraser, Geometry of the steady state approximations: perturbation and accelerated convergence method, J. Chem. Phys. 93 (1990) 1072–1081.
[13] H. Kaper, T. Kaper, Asymptotic analysis of two reduction methods for systems of chemical reactions, Physica D 165 (2002) 66–93.
[14] M. Davis, R. Skodje, Geometric investigation of low-dimensional manifolds in systems approaching equilibrium, J. Chem. Phys. A111 (1999) 859–874.
[15] M. Roussel, Forced-convergence iterative schemes for the approximation of invariant manifolds, J. Math. Chem. 21 (1997) 385.
[16] J. Nafe, U. Maas, A general algorithm for improving ILDMs, Combust. Theory Model. 6 (2002) 697–709.
[17] S. Lam, D. Goussis, Understanding complex chemical kinetics with computational singular perturbation, Proc. Comb. Inst. 22 (1988) 931.

[18] S. Lam, D. Goussis, Conventional asymptotics and computational singular perturbation for simplified kinetics modelling, in: M. Smooke (Ed.), Reduced Kinetic Mechanisms and Asymptotic Approximations for Methane-Air Flames, Springer Lecture Notes, 1991, p. 227.
[19] S. Lam, Using CSP to understand complex chemical kinetics, Combustion Science and Technology 89 (1993) 375–404.
[20] S. Lam, D. Goussis, The CSP Method for Simplifying Kinetics, International Journal of Chemical Kinetics 26 (1994) 461–486.
[21] S. Lam, Reduced chemistry modeling and sensitivity analysis, in: Lecture Notes for Aerothermochemistry for Hypersonic Technology, 1994–1995 Lecture Series Programme, Von Karman Institute for Fluid Dynamics, 1995, p. 3.
[22] D. Goussis, S. Lam, A study of homogeneous methanol oxidation kinetic using CSP, Proc. Comb. Inst. 24 (1992) 113–120.
[23] A. Zagaris, H. Kaper, T. Kaper, Analysis of the CSP reduction method for chemical kinetics, in: SIAM Conference on Applications of Dynamical Systems, Snowbird, Utah, May 27–31, 2003.
[24] U. Maas, S. Pope, Implementation of simplified chemical kinetics based on intrinsic low-dimensional manifolds, Proc. Comb. Inst. (1992) 103–112.
[25] K. Xiao, D. Schmidt, U. Maas, Pdf simulation of turbulent non-premixed CH_4/H_2–air flames using automatically simplified chemical kinetics, Proc. Comb. Inst. 27 (1998) 1073–1080.
[26] T. Blasenbrey, U. Maas, ILDMs of higher hydrocarbons and the hierarchy of chemical kinetics, Proc. Comb. Inst. 28 (2000) 1623–1630.
[27] A. Massias, D. Diamantis, E. Mastorakos, D. Goussis, An algorithm for the construction of global reduced mechanisms with CSP data, Combust. Flame 117 (1999) 685–708.
[28] T. Lovas, D. Nilsson, F. Mauss, Automatic reduction procedure for chemical mechanisms applied to pre-mixed methane/air flames, in: Proc. Comb. Inst., 2000, pp. 1809–1817.
[29] T. Lu, Y. Ju, C. Law, Complex CSP for chemistry reduction and analysis, Combust. Flame 126 (2001) 1445–1455.
[30] M. Valorani, D. Goussis, Explicit time-scale splitting algorithm for stiff problems: auto-ignition of gaseous-mixtures behind a steady shock, J. Comput. Phys. 168 (2001) 1–36.
[31] M. Valorani, H. Najm, D. Goussis, CSP analysis of a transient flame vortex interaction: time scales and manifolds, Combust. Flame 134 (2003) 35.
[32] S.R. Tonse, N. Moriarty, N. Brown, M. Frenklach, PRISM: piecewise reusable implementation of solution mapping. An economical strategy for chemical kinetics, Israel J. Chem. 39 (1999) 97–106.
[33] S. Pope, Computationally efficient implementation of combustion chemistry using in situ adaptive tabulation, Combust. Theory Model. 1 (1997) 41–63.
[34] J. Lee, H. Najm, M. Frenklach, M. Valorani, D. Gousiss, Towards a CSP and PRISM tabulation based adaptive chemistry model, in: Western States Section/Combustion Institute, The Combustion Institute, 2004.
[35] M. Hadjinicolaou, D. Goussis, Asymptotic solution of stiff PDEs with the CSP method – the reaction diffusion equation, SIAM J. Sci. Comput. 20 (1999) 781.
[36] A. Householder, The Theory of Matrices in Numerical Analysis, Dover Publications, New York, 1975.
[37] G. Stewart, Introduction to Matrix Computations, Academic Press, London, England, 1973.
[38] A. Jennings, J.M. Keown, Matrix Computation, Wiley, Chichester, UK, 1992.
[39] R. Skodje, M. Davis, Geometric simplification of complex kinetic systems, J. Chem. Phys. A 105 (45) (2001) 10356.
[40] K. Mease, S. Bharadwaj, S. Iravanchy, Timescale analysis for nonlinear dynamical systems, AIAA J. Guidance Control Dynamics 6 (2) (2003) 318.